JACS
JOURNAL OF THE AMERICAN CHEMICAL SOCIETY

Article

pubs.acs.org/JACS

Probing Ligand Exchange in the P450 Enzyme CYP121 from *Mycobacterium tuberculosis*: Dynamic Equilibrium of the Distal Heme Ligand as a Function of pH and Temperature

Andrew J. Fielding, Kednerlin Dornevil, Li Ma, Ian Davis, and Aimin Liu*

Department of Chemistry, University of Texas at San Antonio, San Antonio, Texas 78249, United States

Supporting Information

ABSTRACT: CYP121 is a cytochrome P450 enzyme from *Mycobacterium tuberculosis* that catalyzes the formation of a C−C bond between the aromatic groups of its cyclodityrosine substrate (cYY). The crystal structure of CYP121 in complex with cYY reveals that the solvent-derived ligand remains bound to the ferric ion in the enzyme−substrate complex. Whereas in the generally accepted P450 mechanism, binding of the primary substrate in the active-site triggers the release of the solvent-derived ligand, priming the metal center for reduction and subsequent O_2 binding. Here we employed sodium cyanide to probe the metal−ligand exchange of the enzyme and the enzyme−substrate complex. The cyano adducts were characterized by UV−vis, EPR, and ENDOR spectroscopies and X-ray crystallography. A 100-fold increase in the affinity of cyanide binding to the enzyme−substrate complex over the ligand-free enzyme was observed. The crystal structure of the [CYP121(cYY)CN] ternary complex showed a rearrangement of the substrate in the active-site, when compared to the structure of the binary [CYP121(cYY)] complex. Transient kinetic studies showed that cYY binding resulted in a lower second-order rate constant ($k_{on\ (CN)}$) but a much more stable cyanide adduct with 3 orders of magnitude slower $k_{off\ (CN)}$ rate. A dynamic equilibrium between multiple high- and low-spin species for both the enzyme and enzyme−substrate complex was also observed, which is sensitive to changes in both pH and temperature. Our data reveal the chemical and physical properties of the solvent-derived ligand of the enzyme, which will help to understand the initial steps of the catalytic mechanism.

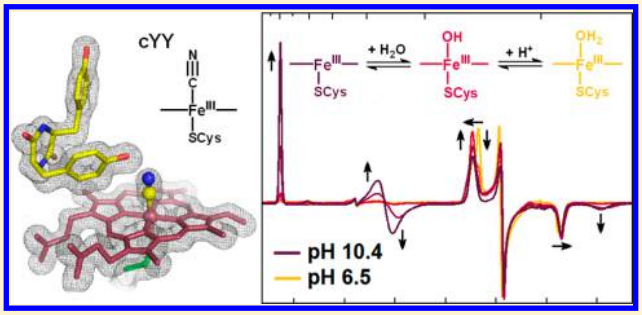

INTRODUCTION

Mycobacterium tuberculosis is a slow-growing bacterium with a waxy cellular membrane.[1] *M. tuberculosis* can effectively evade the host immune system by living inside macrophages themselves, where once engulfed, tuberculosis inhibits acidification of the phagosome and fusion between the phagosome and the lysosome.[2,3] Yet, it does not inhibit the fusion of nutrient field vesicles with the phagosome enabling the bacteria to grow and reproduce within the macrophage. Primary *M. tuberculosis* infections typically affect the lungs (pulmonary tuberculosis (TB)), where the host immune system, in an attempt to control the infection form granulomas around the infection accompanied by caseous tissue necrosis and later calcification, leading to severe tissue damage.[4] Symptoms of TB include prolonged fever, unproductive cough, malaise, and weight loss. Tuberculosis can spread to other tissues, infecting the liver, spleen, kidney, brain, and bones, or to other hosts by coughed-up, TB-containing aerosols.[5] The thick lipid membrane of TB also blocks uptake of antibiotics and allows TB to further avoid desiccation, adding to its virulence.[1] Emerging multi-drug-resistant tuberculosis (MDR-TB) strains, resistant to the first-line anti-tuberculosis medications (isoniazid, rifampin, streptomycin, pyrazinamide, and ethambutol), have further complicated the treatment and spread of TB.[6] In part due to the high cost, negative side effects, and long or poorly monitored treatment, many individuals stop treatment before the infection has cleared, increasing the occurrence of MDR-TB strains.[7−9] Current efforts are focused on developing new drugs with potent anti-mycobacterial activity.

Sequencing the genome of *M. tuberculosis* led to the identification of 20 different cytochrome P450 enzymes, an unusually large number for a bacterium, suggesting P450s as new potential drug targets to treat TB. One of the P450s of special interest, CYP121 (the product of gene *Rv2276*) was shown to be necessary for *M. tuberculosis* vitality in knock out experiments.[10,11] Later, another protein (the product of gene *Rv2275*) was identified in the same operon as CYP121, which catalyzes the ATP-dependent formation of the diketopiperizine ring of cyclodityrosine (cYY, cyclo(L-Tyr-L-Tyr) or 3,6-bis(4-hydroxybenzyl)piperazine-2,5-dione), from its L-tyrosyl-tRNA substrate.[11−13] It was found that CYP121 can catalyze the intramolecular formation of a C−C bond between the two aryl groups of cYY by a *b*-type heme center to form the product, mycocyclosin (Scheme 1).[14] This is an intriguing trans-

Received: August 24, 2017
Published: November 1, 2017

DOI: 10.1021/jacs.7b08911
J. Am. Chem. Soc. 2017, 139, 17484−17499

formation for P450 enzymes, which are mostly known for their ability to hydroxylate C−H bonds of their substrates.

Scheme 1. CYP121-Mediated Chemical Reaction Showing Substrate Cyclodityrosine (cYY) and Product Mycocyclosin (Top Panel) and a Schematic Representation of the Active Site of the Enzyme−Substrate Complex (from PDB Entry 3G5H)[a]

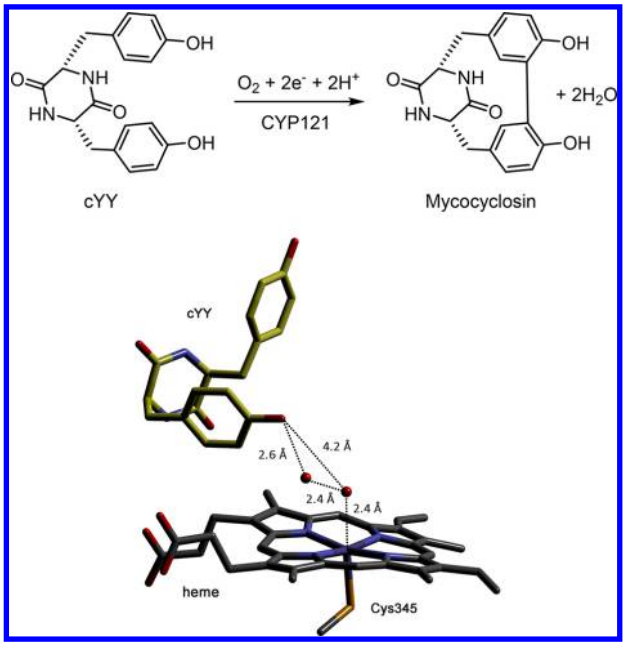

[a]The heme prosthetic group (*b*-type) is bound to the protein through Cys345. cYY binds to the distal heme pocket with one of the tyrosyl groups pointing to the Fe center, forming an H-bonding network with two ordered water molecules.

For reasons still unknown, such a chemical transformation is essential for the survival of the *M. tuberculosis* pathogen. Because of its apparent biomedical significance, previous studies have focused on searching for inhibitors. In our recent study, we found that peracetic acid can oxidize the CYP121-cYY complex via a peroxide shunt mechanism, in which we observed the rapid formation of a probable ferric alkyl-peroxo species.[15] In the later steps of the reactions it catalyzes, CYP121 functions more like a peroxidase than a typical P450.[15] We noticed that, from the very first reaction step, CYP121 does not follow the general P450 chemical mechanism. In the generally accepted mechanism of P450 enzymes, binding of the primary organic substrate results in release of the axial water ligand. This step creates an open coordination site at the iron ion, triggering a spin conversion of the heme from low-spin to high-spin and facilitates iron reduction and subsequent O_2 binding and activation (Scheme 2).[16−18] However, previous EPR and X-ray crystallization studies reveal that this is not the case for ferric form of CYP121 (**E**), and even more confusingly, the EPR and UV−vis data do not agree with each other with regards to spin-state changes induced by the binding of its primary organic substrate.[14] The crystal structures of the [Fe(III)-CYP121-(cYY)] (enzyme−substrate, or **ES**) complex[14] shows that the solvent-derived ligand remains bound to the iron ion as shown in the ligand-free CYP121 structure,[19] which, based on the general P450 catalytic mechanism, should be displaced due to substrate binding-induced structural changes at the enzyme

Scheme 2. General Catalytic Mechanism of Cytochrome P450 Enzymes[a]

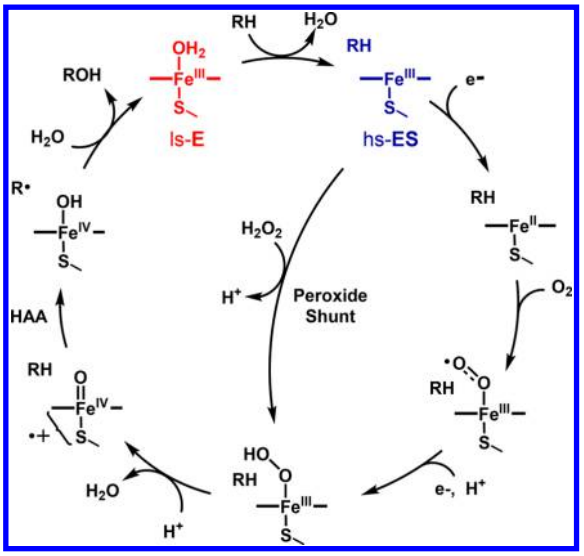

[a]HAA = hydrogen atom abstraction.

active site.[16] The UV−vis data published suggest a spin transition due to binding of the substrate, but the previous EPR studies do not show the low-spin to high-spin transition.[14,20,15] Here, we apply structural, spectroscopic, and kinetic experiments to investigate the equilibria among various heme states as a function of pH and temperature. We also investigated the rate of metal-ligand exchange using the diatomic molecule, NaCN. Our results reconcile the discrepancies mentioned above and provide important insights into the early steps of the CYP121 catalytic mechanism.

MATERIALS AND METHODS

Enzyme Preparation. The cloning and expression of CYP121 and chemical synthesis of cYY were described elsewhere.[15] CYP121 protein was purified as previously reported with some minor modifications. A 200 mL LB media culture containing kanamycin (20 μM) was grown overnight in an incubator at 220 rpm and 37 °C, from colonies picked from an LB/kanamycin agar plate. The next morning the starter culture was used to inoculate 22, 1 L LB/kanamycin cultures. The 1 L cultures were grown at 37 °C until an $OD_{600\ nm}$ of ∼0.3 was reached, at which point, the cultures were supplemented with δ-aminolevulinic acid (300 μM) and iron(II) ammonium sulfate (35 μM). The cultures were then allowed to grow for an additional 20 min ($OD_{600\ nm}$ of ∼0.6) before protein expression was induced with the addition of isopropyl β-D-1-thiogalactopyranoside (400 μM). The incubation temperature was then decreased to 28 °C, and the cultures were grown overnight.

The following day the cells were harvested by centrifugation (8000*g* for 20 min). The cell paste was then suspended in 50 mM lysis buffer (50 mM monobasic potassium phosphate buffer (KPi), pH 8.0, 300 mM NaCl) and passed through an LS-20 cell disrupter (Microfluidics). The lysate was then clarified by centrifugation (2 × 27000*g* for 30 min). The cell lysate was loaded on to a Talon metal affinity column preloaded with $Co(II)Cl_2$. The column was rinsed with buffer containing 50 mM imidazole (50 mM KPi, pH 8.0, 300 mM NaCl) to remove any non-specifically bound protein. The protein was eluted by running a gradient from 50 mM to 125 mM imidazole over 200 mL. Fractions containing CYP121 were pooled and concentrated using an Amicon concentrator with 10 kDa membrane. The protein was then buffer exchanged into 50 mM Tris-HCl buffer pH 7.6 with 5% glycerol, to remove imidazole, by running the protein down a Sephadex G-25 (2.6 × 28 cm) desalting column. The fractions

DOI: 10.1021/jacs.7b08911
J. Am. Chem. Soc. 2017, 139, 17484−17499

containing CYP121 were again pooled and concentrated. The protein concentration was determined using $\varepsilon_{280\ nm}$ = 26 500 M^{-1} cm^{-1}, while the heme concentration was determined using the Soret band, $\varepsilon_{416\ nm}$ = 110 000 M^{-1} cm^{-1}.[10] The purified protein was concentrated to between 0.6 and 1.2 mM in protein. The heme occupancies averaged between 45−56% [heme]/[protein] as determined by UV−vis. The purified protein was then flash frozen in liquid nitrogen and stored at −80 °C until required.

EPR of Fe(III)-CYP121: E, ECN, ES, and ESCN Complexes. EPR samples of **E** and **ES** were prepared by incubating samples of 0.38 mM Fe(III)-CYP121 [heme], in 150 mM 2-[4-(2-hydroxyethyl)piperazin-1-yl]ethanesulfonic acid (HEPES) buffer, pH 7.6 at 21 °C; 1.3 mM cYY was added to form the **ES** complex (1.6% [dimethyl sulfoxide (DMSO) v/v] final). Samples were then frozen by either slowly submerging the EPR tube in liquid nitrogen, or by rapidly submerging into either an acetone/dry ice slurry, isopentane/liquid nitrogen slurry, or in liquid ethane over a liquid nitrogen bath. EPR samples of the cyanide adducts (**E**CN and **ES**CN) were prepared by incubating the **E** or **ES** complexes with 55 mM NaCN in an X-band EPR tube for 20 min at 21 °C and slowly submerging samples in liquid nitrogen. EPR spectra were collected at 4.5 K and 25 mW microwave power or at 20 K and 2.0 mW microwave power using a Bruker E560 X-band spectrometer at 9.6 GHz microwave frequency with a dual mode resonator at 100 kHz modulation frequency equipped with a cryogen-free 4 K temperature system as described in earlier.[15] The *g* values reported in text were obtained by inspecting the EPR line shape and by comparing the EPR spectra for multiple samples in buffers ranging from pH 6.5 to 10.4. Due to the overlapping features of the different species, the specific *g* values for each species were determined at the specified pH by analyzing the resonances of the EPR spectra.

pH Dependency Experiments. The following buffers were used for pH-dependent experiments or as indicated for each individual experiment. Buffers consisted of either 150 mM 2,2-bis(hydroxymethyl)-2,2′,2″-nitrilotriethanol (Bis-Tris), pH 6.5; 150 mM HEPES, pH 7.5; 150 mM 2-amino-2-(hydroxymethyl)-1,3-propanediol (Tris-base), pH 8.5; 150 mM *N*-cyclohexyl-2-aminoethanesulfonic acid (CHES), pH 9.5; 150 mM boric acid, pH 10.0; or 75 mM NaPi/Na_2Pi with 75 mM boric acid, pH 10.4.

pH Dependence of E, ES: EPR Spectroscopy. Concentrated solutions of CYP121 were buffer exchanged into 150 mM buffered solutions described above by adding 0.8 mL of 120 μM heme concentration of CYP121 diluted with 0.5 mL of the new buffer to a G-25 desalting column pre-equilibrated with the desired buffer and then eluting the protein. The eluted protein was then concentrated by filter centrifugation with a 10 kDa spin filter concentrator. Alternately, the protein was buffer exchanged by diluting the sample 6-fold with the desired buffer and then re-concentrating the sample using a 10 kDa spin concentrator to roughly the initial volume and repeating this cycle five times. The final concentration of heme was then measured by UV−vis at pH 7.5 ($\varepsilon_{418\ nm}$ = 110 000 M^{-1} cm^{-1}). The enzyme−substrate complex was then formed by slowly adding 80 mM cYY dissolved in DMSO to the enzyme (~330 μM [heme]), to a final concentration of 1.3 mM [cYY], and 1.6% DMSO. Samples where frozen by rapid submersion into a dry ice acetone bath at −78 °C. Whenever possible, the cYY was added to the buffer prior to the addition of CYP121 to avoid precipitating the protein with the initial local high concentration of DMSO. When preparing EPR samples of the enzyme−substrate complex, the cYY was added very slowly to the protein while gently stirring. The final heme concentration, as determined by UV−vis, were used to normalize the intensity of the EPR spectra of samples prepared at different pH values, for differences in heme concentrations.

cYY Titrations of Fe(III)-CYP121. Titration experiments were performed by first diluting CYP121 from concentrated stock solution to 150 mM buffers of various pHs described above. The titration experiment was performed by adding cYY from concentrated stock solutions (10 or 80 mM), of cYY dissolved in DMSO, to a 1.0 mL solution of CYP121 (10 μM heme concentration). The DMSO concentration at the end of the cYY titrations was <3%.[20] Spectra of the samples were acquired after each successive addition of cYY on a PerkinElmer Lambda 25 UV/vis spectrophotometer. The formation of the **ES** complex was monitored by following the amplitude difference between 386 and 419 nm over the course of the titration. The amplitude change was then plotted against the corresponding cYY concentration, and the data were fitted using nonlinear regression to a hyperbolic equation (eq 1) using the program SigmaPlot. Data were then graphed to show percent fraction bound (θ%, eq 2).

$$\Delta\mathrm{Abs} = \frac{\Delta\mathrm{Abs}[\mathrm{Ligand}]}{K_\mathrm{D} + [\mathrm{Ligand}]} \quad (1)$$

$$\theta,\ \% = \frac{\Delta\mathrm{Abs}}{\Delta\mathrm{Abs}_{max}} \quad (2)$$

NaCN Titrations of Fe(III)-CYP121 Enzyme and [Fe(III)-CYP121(cYY)] Enzyme−Substrate Complex. For titrations of Fe(III)-CYP121 (1 mL, 10 μM heme concentration), the protein was diluted into 150 mM buffers of various pHs described above and placed into a rectangular quartz cuvette (1 cm). The 150 mM buffer proved necessary for titration of the Fe(III)-CYP121 with cyanide, to buffer the reaction at high NaCN concentrations. The enzyme−substrate complex was prepared for titration experiments by incubating 10 μM heme concentration with 0.67 mM cYY, from an 80 mM cYY stock solution dissolved in DMSO. The cYY was added to the buffer prior to the addition of the CYP121 to avoid precipitating the protein, as the protein precipitates in high DMSO concentrations.[20] NaCN was added to the cuvette using 1−5 μL additions from either 10 or 100 mM fresh stock solutions of NaCN. NaCN binding was very slow taking ~20 min to equilibrate between additions of NaCN at room temperature. Equilibration with each successive addition of NaCN was monitored by following the decrease in absorbance at 408 or 394 nm following the decay of the **E** or **ES** complex, respectively, or by monitoring the formation of the cyanide adducts at 440 nm. The titration data were then fitted as described above using nonlinear regression to determine the dissociation constant (K_D) value (eqs 1 and 2).

Determination of the Extinction Coefficient and pK_a for Cyclodityrosine (cYY). cYY was synthesized as previously reported by Belin et al.[14] The extinction coefficient of cYY was determined by first preparing three 80 mM solutions of cYY (fw = 326.35 g/mol) dissolved in DMSO. From these concentrated stock solutions, 70 μM solutions of cYY were then prepared (in triplicate for each stock solution) in buffered solutions ranging from pH 6.0 to 12.5, and the UV−vis spectra were acquired at each pH value. The spectra of solutions at each pH were then averaged. The formation of monoanionic cYY could be followed at 292 nm at increasingly higher pH values. The intensity of the 292 nm absorbance band was plotted against pH and then fitted using nonlinear regression to a sigmoidal equation (eq 3) to determine the pK_a, where A_{292} is the measured absorbance at 292 nm, $\Delta\mathrm{Abs}_{max}$ is the maximum measured change in intensity at 292 nm, pH is determined by the experimental buffer, and *b* is the steepness of the curve.

$$A_{292} = \frac{\Delta\mathrm{Abs}_{max}}{1 + e^{-(\mathrm{pH}-\mathrm{p}K_a/b)}} \quad (3)$$

NaCN Binding Stopped-Flow Experiments. Stopped-flow experiments were carried out on an Applied Photophysics SX20 stopped-flow system, using either a photodiode array or a photomultiplier tube detector to obtain multi-wavelength or single-wavelength kinetic data. Reactions were carried out by rapidly mixing solutions of either Fe(III)CYP121 (9 μM CYP121 [heme] after mixing) or the [Fe(III)CYP121(cYY)] enzyme−substrate complex with NaCN and then monitoring the formation of the cyanide adduct at 440 nm. The enzyme−substrate complex was preformed by incubating 20 μM CYP121 [heme] with 2 mM cYY (2.5% v/v DMSO), resulting in 10 μM CYP121 [heme] and 1 mM cYY after mixing with NaCN solution. For kinetic experiments the NaCN concentration was varied between 1.5 and 30 mM NaCN after mixing. The experiments were carried out in 150 mM HEPES buffer, pH 7.5 at

DOI: 10.1021/jacs.7b08911
J. Am. Chem. Soc. 2017, 139, 17484−17499

21 °C. Single-wavelength kinetic traces were fitted with single, double, or triple summed exponential equations (eqs 4–6).

$$\mathrm{Abs}(t) = a_1 e^{-k_1 t} + c \quad (4)$$

$$\mathrm{Abs}(t) = a_1 e^{-k_1 t} + a_2 e^{-k_2 t} + c \quad (5)$$

$$\mathrm{Abs}(t) = a_1 e^{-k_1 t} + a_2 e^{-k_2 t} + a_3 e^{-k_3 t} + c \quad (6)$$

CW-ENDOR of Fe(III)CYP121, [Fe(III)CYP121(CN)], [Fe(III)-CYP121(cYY)], and [Fe(III)CYP121(cYY)CN] Complexes. ENDOR samples were prepared with concentrated protein with 1.0–1.3 mM heme concentration. The enzyme–substrate complexes were prepared by the addition of 1.7 mM cYY, while the cyanide complexes were formed by incubating the samples with 50 mM potassium cyanide-^{13}C obtained from Sigma-Aldrich. EPR samples for ENDOR experiments were frozen by slowly submerging EPR tubes in liquid nitrogen to maximize the yield of the low-spin species for subsequent characterization.

ENDOR spectra were acquired using a Bruker E560 X-band spectrometer at 9.4 GHz microwave frequency with 25 kHz modulation frequency in an EN 801 cavity. ^{1}H ENDOR spectra were acquired in frequency modulated (FM) mode at saturating power and temperature conditions at ∼20 K, 25.2 mW microwave power, and 68–78 W radio power, with 100 kHz frequency modulation depth. ENDOR spectra shown in figures are from in-phase and out-of-phase signals of the second harmonic, resulting in absorption-like spectra. The ENDOR spectrum of a nucleus with $a_I = 1/2$, with a single paramagnetic center, consists of a doublet with frequencies $\nu_\pm$, given by[21]

$$\nu_\pm = |\nu_N \pm A/2| \quad (7)$$

Here, ν_N is the nuclear Larmor frequency, and A is the orientation-dependent hyperfine coupling constant of the nucleus. The doublet is centered at the Larmor frequency and separated by A when $\nu_N > |A/2|$, as in the case for ^{1}H spectra.

Crystallization of the CYP121 Ternary Complex ESCN and X-ray Data Collection. Crystals of CYP121 were obtained using the hanging drop method. The His$_6$-tagged CYP121 was cleaved using the Thrombin Cleavage Kit (Sigma-Aldrich) prior to crystallization, and the enzyme was buffer-exchanged into 50 mM Tris-HCl pH 7.4. The crystallization conditions consisted of 100 mM MES buffer pH 5–6.5, 1.75–2.5 M ammonium sulfate, and 400 μM cYY at 4 °C in a vibration-free crystallization refrigerator. The protein was mixed in a 1:1 ratio with the reservoir solution for a total drop volume of 3 μL. The CYP121 crystals appeared within 1 week. To obtain the cyanide complex, the crystals were transferred to a new buffer solution containing 100 mM Tris-HCl pH 8.0, 2 mM ammonium sulfate, and 50 mM sodium cyanide and allowed to soak for 2 h. The crystals were then mounted onto a loop and stored in liquid nitrogen under protection of a cryoprotectant consisting of the mother liquor and 20% glycerol prior to data collection.

X-ray diffraction data were collected at the Stanford SSRL 9-2 beamline. Diffraction data were collected at 1.0 Å wavelength using a Pilatus detector, and the crystal was kept under a nitrogen stream at 100 K. The diffraction data were processed using the software HKL-2000.[22] Structures were solved by molecular replacement using (PDB entry 1N40)[19] as the search template and the Phaser-MR[23] software in the PHENIX program package.[24] All ligands including the heme, cyanide, and cYY were observed with 100% occupancy within the enzyme active site after data collection, model building, and refinement. Water molecules were added during the final refinement steps of model building. The software Coot[25] and PHENIX[24] were used for model building and refinement.

Hazardous Procedures. ***Caution:*** Potassium/sodium cyanide is a highly toxic chemical. Exposure to it can lead to rapid death. Cautions must be taken in preparing the stock solution, during use, and in disposing of waste. Sodium cyanide solutions can generate highly toxic hydrogen cyanide gas (pK_a = 9.3) when in acidic or neutral pHs. Cyanide waste was segregated from other lab waste and further treated by the addition of NaOH.[26]

RESULTS

pH Dependence of Species Observed by EPR of Fe(III)CYP121 and [Fe(III)CYP121(cYY)]. The EPR spectra of the Fe(III)CYP121 and the [Fe(III)CYP121(cYY)] (hereafter referred as **E** and **ES**, respectively) complex have been reported by Belin et al. and us.[14,15,27] At pH 7.2 (50 mM Tris-maleate) and with a high modulation amplitude (16 G), only a single low-spin species for the as-isolated enzyme was reported (g = 2.49, 2.26, and 1.89).[14] In our initial efforts to purify CYP121 we observed two distinct low-spin (S = 1/2) signals when measured with 6 G modulation amplitude in the as-isolated protein at pH 7.4 (50 mM Tris-HCl).[15] At low temperature and high microwave powers (4.5 K and 25.2 mW), a small population of a high-spin heme (S = 5/2) was also observed.[15] As our EPR experiments were performed on a His$_6$-tagged protein, purified using a cobalt–metal affinity column, eluted using an imidazole gradient, we performed additional control experiments demonstrating that the as-isolated protein was free of contaminating imidazole (Figure S1), showing that the second low-spin species is not an artifact of the purification process.

The ratio of the two low-spin species proved to be pH-dependent (Figure 1). Spectra of low-spin species acquired under non-saturating conditions (Figure S2) for quantification can be found in Figure S3. At pH 6.5 there is a mixture of the two low-spin species with the less rhombic signal dominating (termed ls-**E**1, g = 2.44, 2.26, and 1.91). As the pH is raised from 6.5 to 8.5 the intensity of the EPR signal from ls-**E**1 species decreases with the concurrent increase in the signal of the other low-spin signal (ls-**E**2, g = 2.49, 2.25, and 1.89), with isosbestic points observed at g = 2.47 and 1.90, indicating a clean conversion from ls-**E**1 to ls-**E**2. The pH dependence of these two low-spin species suggest that ls-**E**2 is the conjugate base of ls-**E**1, with an apparent pK_a of ∼7.5. The low-spin species observed in the EPR spectra of **ES** exhibits more subtle shifts in the g values with pH (Figure 1A and Figure S3), where the EPR signal gets steadily more rhombic as the pH is increased from pH 6.5 (ls-**ES**1, g = 2.47, 2.25, and 1.90) to 10.4 (ls-**ES**2, g = 2.46, 2.24, and 1.91) with an apparent pK_a of ∼8.0.

The high-spin ferric EPR signal (S = 5/2), for both hs-**E** and hs-**ES**, can be best observed at 4.5 K and 25.2 mW (Figure S2).[15] Substrate binding perturbs the high-spin species as can be observed in a shift in the low-field signal from g = 8.01 to 8.13 upon addition of cYY at pH 6.5. Only a very subtle change in the rhombicity of the high-spin species is observed upon increasing the pH from 6.5 to 10.4 for both the hs-**E** and hs-**ES** (Figure 1 and Table 1), which is best perceived as a small shift in the low-field signal from g = 8.01 to 7.99 for the hs-**E**, and from g = 8.13 to 8.06 for hs-**ES**. The intensity of the hs-**ES** signal is not greatly affected by pH, while the intensity of hs-**E** increases substantially above pH 8.5 (Figure 1), with a concurrent decrease in the intensity of the ls-**E**2, suggesting a spin-state conversion between the ls-**E**2 and hs-**E** above pH 8.5. These experiments clearly show multiple low- and high-spin species for both **E** and **ES** which are in equilibrium with each other. It should be noted that the pH-dependent experiments were limited to pH values between 6.5 and 10.4 due to protein precipitation under more acidic or basic conditions as previously reported by Dunford et al.[28]

DOI: 10.1021/jacs.7b08911
J. Am. Chem. Soc. 2017, 139, 17484–17499

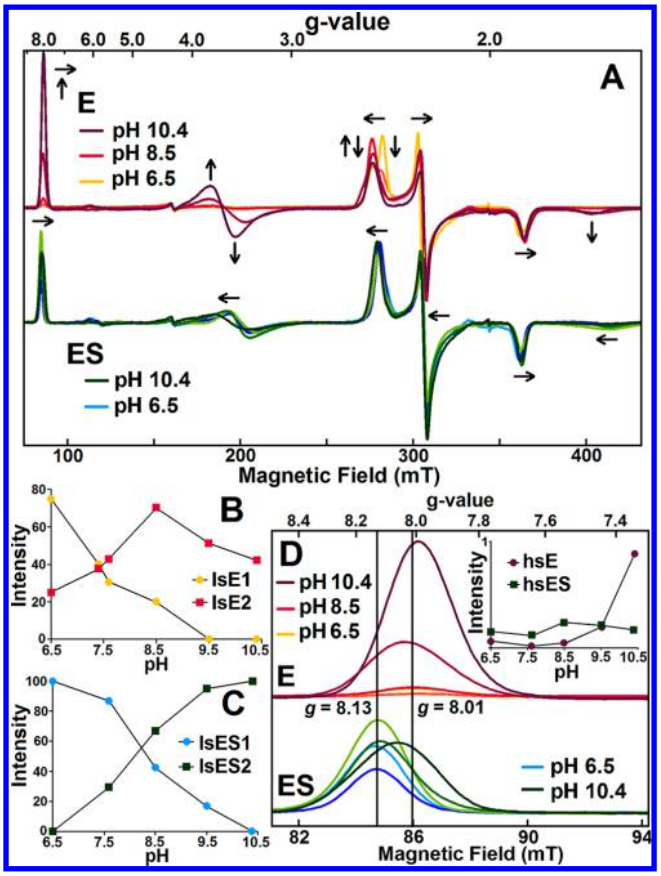

Figure 1. EPR spectra of **E** and **ES**, prepared in buffers ranging from pH 6.5 to 10.4 (A). Comparison of relative intensity of low-spin species for ls-**E**1 and ls-**E**2. Arrow shows the direction of change in the different observed EPR features upon increasing the pH from 6.5 to 10.4. (B) and the ls-**ES**1 and ls-**ES**2 (C) as a function of pH. Closer view of g = 8 signals from S = 5/2 species for better comparison (D). Lines are drawn at g = 8.01 and 8.13 as guides. The inset in (D) shows the signal intensity of hs-**E** and hs-**ES** with pH. EPR samples were prepared by rapid submersion in a dry ice−acetone bath at −78 °C. The EPR spectra were collected at 4.5 K, 9.6 GHz microwave frequency, 25.2 mW, 100 kHz modulation frequency, and 6 G modulation amplitude. Spectra have been normalized to account for the different heme concentration in each sample for better comparison of the intensity of each species.

Temperature Effects on the Equilibrium between High-Spin and Low-Spin Species. During the course of EPR sample preparations it was noticed that the ratio of high- to low-spin species for **E** and **ES** varied from sample to sample. Previous UV−vis, EPR, and Mössbauer spectroscopes studies with other P450 isoforms have shown that there is often a temperature-dependent equilibrium between high- and low-spin heme, in which the high-spin species is favored at higher temperatures.[18,29−31] We found that samples prepared by slowly submerging the EPR tube in liquid nitrogen, to avoid breaking the EPR tube due to rapidly expanding water in the sample, resulted in relatively little to no S = 5/2 high-spin heme (Figure 2). Alternatively, samples frozen by rapid submersion in a liquid nitrogen/isopentane bath (−160 °C) contained a larger fraction of high-spin heme, and samples frozen rapidly in liquid ethane (−183 °C) showed both a significant increase in the high-spin heme and a decrease in the intensity of the low-spin heme. The observation that a significant amount of high-spin species can only be detected when the sample is frozen rapidly suggests that there is an equilibrium between the five-coordinate high-spin heme and the six-coordinate low-spin heme at room temperature. The effect of freezing speed on the ratio of high-spin to low-spin heme was observed by EPR for both **E** and **ES** at both low (pH 7.4, Figure 2) and high pH (10.4, Figure S4). When samples are frozen slowly in liquid nitrogen, they are allowed to cool relatively slowly to 0 °C prior to freezing, with enough time for the high- and low-spin species to re-equilibrate before the sample becomes frozen and/or cools completely to liquid nitrogen temperatures (−196 °C). Conversely, the samples cooled more rapidly in either isopentane or liquid ethane had less time for the high- and low-spin species to re-equilibrate before the sample cooled below the solvent glass temperature.[18] The higher population of high-spin heme observed by EPR upon rapid freezing is more consistent with the Type I spectral changes observed by UV−vis upon cYY binding at room temperature, where a blue-shift of the heme Soret band from 416 to 395 nm is observed,[14,15,27] which suggests displacement of the solvent-derived ligand upon substrate binding to yield a five-coordinate high-spin heme.[17,18]

In UV−vis experiments of **ES**, with 670 μM cYY, ∼30 times the K_D value for cYY (19.4 ± 0.6 μM cYY, pH 7.2),[20] a shoulder at 416 nm remains, suggesting an equilibrium between the five-coordinate high-spin heme and six-coordinate low-spin heme species at room temperature. In EPR samples that are frozen rapidly, this spin-state equilibrium can be frozen in place and observed. Consistent with the observed spin-state transition observed by EPR, the UV−vis spectra of **E** shows similar temperature dependence. In the UV−vis spectra of **E** collected at 4 and 30 °C (Figure S5A), the intensity of the Soret band of **E** decreases at 416 nm upon raising the temperature and is accompanied by an increase in absorbance at 386 nm, suggesting an increase in the population of the five-coordinate high-spin heme at elevated temperatures.[32] Only a small increase in absorbance at 416 nm is observed between the spectra of **ES** collected at 30 and 4 °C, which is likely due to a significant increase in the K_D value for cYY at 4 °C or from the poor solubility of cYY in water at low temperatures, resulting in rapid precipitation of the substrate at 4 °C (Figure S5B).

An alternate explanation for the perturbed ratio of high- to low-spin heme for samples frozen at different rates could be due to a decrease in the pK_a of the buffer with temperature, which can result in a significant increase in the pH of the solution as the temperature drops.[33] In the above pH-dependent experiments, it was observed that the ratio of the high- and low-spin species for **ES** showed very little change for samples frozen at comparable rates in a dry ice acetone bath, as a function of pH (Figure 1). Whereas the spectra of **ES** samples frozen rapidly showed a significant increase in the ratio of the high- to low-spin species (Figure 2). Additionally, the ratio of the ls-**E**1 and ls-**E**2 species does not appear to change for samples frozen at different rates as they do with pH (Figure 1), suggesting that the pH of the sample has not been affected significantly by the different freezing rates. The higher yield of the high-spin heme observed in the rapidly frozen samples gives a more accurate picture of the equilibrium between low- and high-spin heme at room temperature and is also more consistent with the UV−vis spectroscopic changes which suggests an increase in the population of high-spin heme upon cYY binding.

NaCN Binds to the Enzyme−Substrate Complex with a Much Higher Affinity than to CYP121. Cyanide binding

DOI: 10.1021/jacs.7b08911
J. Am. Chem. Soc. 2017, 139, 17484−17499

Table 1. EPR Parameters for Species Observed in CYP121 E, ECN, ES and ESCN Samples[a]

CYP121 complex	species and pH	S	g values	E/D	refs
Fe(III)-CYP121, **E**	ls-**E**1, pH 6.5	1/2	2.44, 2.26, 1.91		14, 27
	ls-**E**2, pH 8.5	1/2	2.49, 2.25, 1.89		15
Fe(III)-CYP121, **E**	hs-**E**1, pH 6.5	5/2	8.01, 3.6, 1.6	0.102	15
	hs-**E**2, pH 10.4	5/2	7.99, 3.6, 1.7	0.107	this work
[Fe(III)-CYP121(CN)], **ECN**	**ECN**	1/2	2.58, 2.31, 1.82		this work
[Fe(III)-CYP121(cYY)], **ES**	ls-**ES**1, pH 6.5	1/2	2.47, 2.25, 1.90		14, 15
	ls-**ES**2, pH 10.4	1/2	2.46, 2.24, 1.91		this work
[Fe(III)-CYP121(cYY)], **ES**	hs-**ES**1, pH 6.5	5/2	8.13, 3.5, 1.6	0.099	15
	hs-**ES**2, pH 10.4	5/2	8.06, 3.6, 1.7	0.098	this work
[Fe(III)-CYP121(cYY)CN], **ESCN**	**ESCN**	1/2	2.52, 2.31, 1.84		this work

[a] *g* values for each complex reported here were measured at the specified pH values. *g* values have been rounded to the nearest hundredths or tenths decimal place for the low-spin and high-spin species, respectively. EPR parameters for ls-**E** and ls-**ES** complexes were previously reported at pH 7.2, with 16 G modulation amplitude.[14,27] Parameters for ls-**E**1, ls-**E**2 hs-**E1**, and hs-**ES**1 were previously reported by us at pH 7.4, using 6 G modulation amplitude.[15]

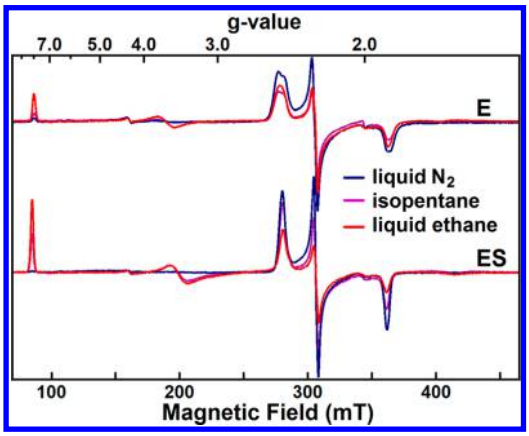

Figure 2. EPR spectra of **E** and **ES** at pH 7.6. Samples prepared initially at 22 °C and then frozen by various methods: (blue) slow submersion in liquid nitrogen, (magenta), rapid submersion in isopentane at −160 °C, (red) rapid submersion in liquid ethane at −183 °C. **ES** was prepared by incubating CYP121(285 μM heme with 1.3 mM cYY. Spectra were collected at 4.5 K, 25.2 mW microwave power, 100 kHz modulation frequency, and 6 G modulation amplitude.

to **E** results in a shift in the heme Soret peak from 416 to 438 nm. Thus, binding of the anionic cyanide ligand to **E** can be followed by UV−vis spectroscopy (Figure 3A). Cyanide binding titration experiments were also performed on **ES** (Figure 3B), resulting in a shift in the Soret band from 394 to 438 nm. These observed spectroscopic changes are consistent with formation of a low-spin Fe(III)-cyanide adduct, **ECN** and **ESCN**, respectively (Table 2).[34−36] The UV−vis spectra of the final **ECN** and **ESCN** complexes are nearly identical between 300 and 900 nm with absorption bands at 368, 438, 562, and 758 nm (Figure 3A,B), suggesting the effect of cYY binding on the electronic structure of the heme center is inaccessible by direct comparison of the absorption spectra. However, the difference spectra (Figure 3C,D) for the titrations show maximum changes in amplitude for the titration of **E** with NaCN at 408 and 440 nm, while the titration of **ES** had maximum changes at 394 and 440 nm.

The NaCN titrations were monitored by following the change in absorbance at 408 nm for the titration of **E**, and 394 nm for titrations of **ES**, upon successive additions of NaCN (Figure 3). At very low NaCN concentrations, the binding of NaCN took 15−90 min to establish equilibrium between additions of NaCN. Titration data were fitted to a hyperbolic function to obtain K_D values and then plotted as percent fraction bound (θ%, Figure S6). **ES** has a much higher affinity for cyanide (K_D^{NaCN} = 83 ± 6 μM), than **E** (K_D^{NaCN} = 8800 ± 300 μM).

NaCN exhibits a 2 orders of magnitude higher affinity for **ES** over **E**, suggesting that binding of the primary substrate (cYY) to the enzyme results in the destabilization of the solvent-derived ligand and/or stabilization of the CN^- ligand. The increased affinity for CN^- upon substrate binding may also suggest an ordered mechanism for CYP121 where cYY would bind prior to O_2 or H_2O_2 during turnover via the peroxide shunt pathway. In our previous study with peracetic acid, we observed accumulation of the probable high-spin Fe(III)-organic peroxide species in rapid freeze-quench studies only in the presence of substrate.[15]

EPR Characterization of ECN and ESCN Complexes. The EPR spectrum of **E** at pH 7.5 exhibits two low-spin species and one high-spin species (see Materials and Methods for details of sample preparations). Addition of cYY results in the conversion of the two low-spin species to a single low-spin species. We found a slight perturbation of the *g* values of the high-spin species at *g* = 8 at various pH's (Table 1).[14,15,27] Upon addition of cyanide to **E** the three species coalesce to form one uniform low-spin ferric cyanide adduct (**ECN**, Figure 4, *g* = 2.58, 2.31, and 1.82). Binding of cyanide to **ES** results in the conversion of the high- and low-spin **ES** species to form a uniform low-spin cyanide adduct (**ESCN**, *g* = 2.52, 2.31, and 1.84), as is expected for this strong field ligand.[16,34,36,37] Nevertheless, a small fraction of the **ECN** species in the **ESCN** EPR spectrum is noticed from the slight shoulders at *g* = 2.58 and 1.82. Though the UV−vis electronic absorption spectra of the **ECN** and **ESCN** species were nearly identical, the EPR spectra of the **ECN** is more rhombic than the **ESCN** species, with a significant shift and slight narrowing of the g_z

DOI: 10.1021/jacs.7b08911
J. Am. Chem. Soc. 2017, 139, 17484−17499

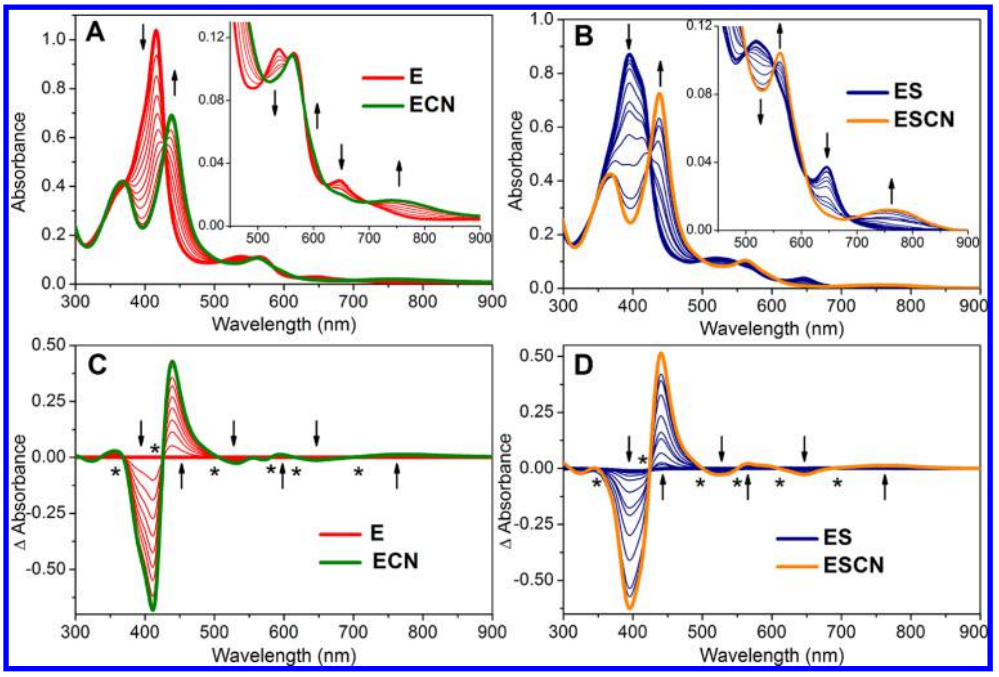

Figure 3. UV−vis titration of (A) **E** (10 μM heme) with NaCN (0−55 mM) to form an orange-colored cyanide adduct, **ECN** in pH 7.5 HEPES buffer (150 mM). (B) Titration of **ES** (10 μM [heme] with 0.67 mM cYY) with NaCN (0−15 mM). (C) Difference spectra subtracting the spectrum for **E** from titration data. (D) Difference spectra subtracting the spectrum of **ES** from titration.

Table 2. UV−Vis Absorbance Spectra Data of Enzyme, Enzyme−Substrate, and Cyanide Complexes

P450 enzyme complex	absorbance bands (nm)						refs
Fe(III)-CYP121, **E**		416		539	565	647	5, 15
[Fe(III)-CYP121(CN)], **ECN**	368		438		562	758	this work
[Fe(III)-CYP121(cYY)], **ES**		394		520	540/547	647	15
[Fe(III)-CYP121(cYY)CN], **ESCN**	368		438		562	758	this work
Fe(III)-CYP101	361	418		538	572		34
[Fe(III)-CYP101(CN)]	365		440		560		34
[Fe(III)-CYP101(cam)]		392		545		643	34
[Fe(III)-CYP101(cam)CN]	366		440		560		34

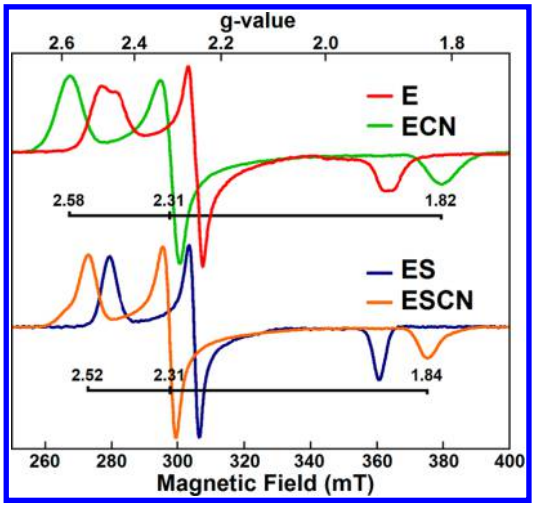

Figure 4. EPR spectra of **E**, **ECN**, **ES**, and **ESCN**, showing low-spin S = 1/2, CN-adducts at pH 7.5. Complexes formed with the addition of 0.95 mM cYY and/or 55 mM NaCN with CYP121 (380 μM heme). The **ECN** and **ESCN** EPR samples were prepared by slowly submerging the samples in liquid nitrogen. Spectra were collected at 20 K, 9.6 GHz microwave frequency, 2 mW microwave power, 100 kHz modulation frequency, and 6 G modulation amplitude.

component, as might be expected if cYY interacts with the axial cyanide ligand.

Stopped-Flow Kinetics Studies of NaCN Binding. To further investigate the different K_D values for NaCN binding to **E** and **ES**, stopped-flow studies were performed to determine the microscopic rate constants (k_{on} and k_{off}) for cyanide binding. The formation of the cyanide-adducts was monitored by following the increase in absorption spectrum at 440 nm upon mixing with NaCN (Figure 5). The final NaCN concentration, after mixing, ranged from 1.5 to 50 mM. In the stopped-flow experiments monitoring NaCN binding to **E** at pH 7.5, equilibrium was rapidly established within ∼10 s (Figure 5A). The binding of NaCN to **ES** was considerably slower, taking 30−500 s for equilibrium to be established (Figure 5B). From the stopped-flow traces for the reaction of **E** and **ES** with 1.5 mM NaCN, it can also be clearly seen that despite the much slower binding of cyanide to **ES** than to **E**, the final yield of the cyanide-adduct is much higher for **ES** (95% **ESCN**) compared to **E** (∼15% **ECN**). This is consistent with the much lower K_D^{NaCN} for **ES**. The observed slower binding of cyanide to **ES** than to **E** is somewhat surprising given the 2 orders of magnitude higher affinity (lower K_D value) of cyanide for **ES** (K_D^{NaCN} = 0.083 ± 0.006 mM) then for **E** (K_D^{NaCN} = 8.8 ± 0.3 mM). In order for cyanide to exhibit a 100-fold higher

DOI: 10.1021/jacs.7b08911
J. Am. Chem. Soc. 2017, 139, 17484−17499

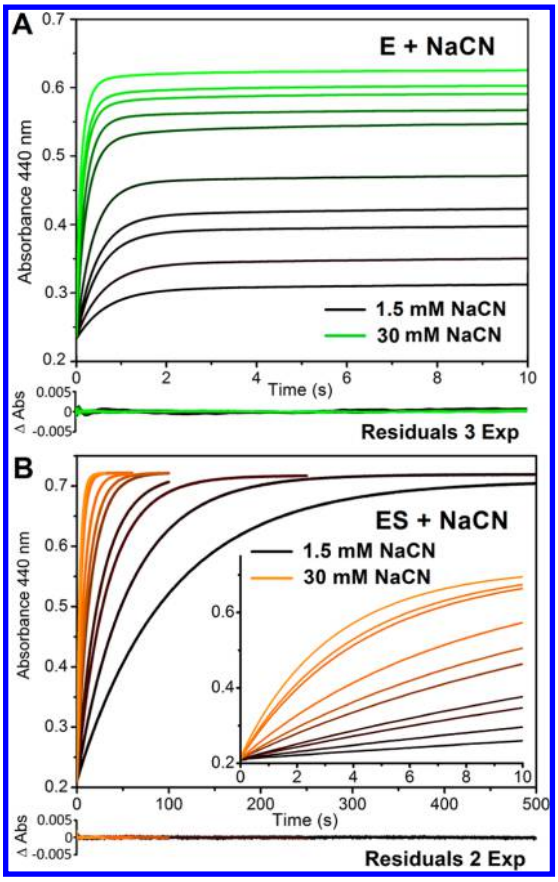

Figure 5. Stopped-flow traces monitoring formation of (A) **E**CN and (B) **ES**CN at 440 nm. Reaction conditions for formation of **E**CN: pH 7.5, 21 °C, 9 μM heme, and NaCN concentration ranging from 1.5 to 30 mM after mixing. **ES** was preformed by incubating **E** with 2 mM cYY. Reaction conditions for formation of **ES**CN: 10 μM heme, 1 mM cYY, and NaCN concentration ranging from 1.5 to 30 mM after mixing. Plots below graphs show residuals from the best fit of kinetic data. Transient data fitted to one, two, or three summed exponential equations (eqs 4–6).

affinity ($K_D = k_{off}/k_{on}$) for **ES** over **E**, yet present an apparent slower cyanide binding rate (k_{on}), the cyanide dissociation rate (k_{off}) would need to have decreased significantly from **ES**CN compared to **E**CN.

The NaCN concentration dependence data can be fitted to give additional insights into the changes in the rates of cyanide binding (k_{on}) and dissociation (k_{off}) between **E** and **E**CN, and **ES** and **ES**CN complexes, respectively. Fitting the stopped-flow traces for NaCN binding to **E** with a single exponential function gave very poor fits to kinetic traces where residuals showed systematic dependence on NaCN concentration. Obtaining a reasonable fitting of the kinetic data for NaCN binding to **E** required fitting with a summed triple exponential function (Figure 5A). The requirement of three exponentials may not be too surprising, given the EPR data, which show one high-spin and two low-spin Fe(III) species in equilibrium with each other for **E**, where each species likely forms the cyanide complex at a different rate.

The plot of the reciprocal relaxation times from triple exponential fitting of the stopped-flow data for NaCN binding to **E** is shown in Figure S7A. The triple exponential fitting gives two reciprocal relaxation times ($1/\tau_1$ and $1/\tau_2$) that exhibit linear concentration dependence with non-zero y-intercepts, while the third ($1/\tau_3$), has a slight parabolic concentration dependence. These data suggest that NaCN binding to the as-isolated enzyme is a complicated process with many different species in relatively slow equilibrium with each other. The parabolic behavior of ($1/\tau_3$) is likely due to its rate becoming indistinguishable from the other two rates at low NaCN concentration. Similarly, the plots from fitting the kinetic data to a double exponential equation (Figure S7B) resulted in $1/\tau_1$, displaying linear concentration dependence, while $1/\tau_2$, had parabolic NaCN concentration dependence. Fitting the data to just a single exponential equation (Figure S7C) resulted in a poor fit of the kinetic data but a plot for $1/\tau_1$ that showed linear concentration dependence with a nonzero y-intercept. These data are consistent with reversible binding of NaCN to **E**, where the slope can give a rough estimate for the second order rate constant ($k_{on} \approx 0.26$ mM^{-1} s^{-1}) associated with NaCN binding. One can then estimate the dissociation rate constant based on the measured K_D value ($K_D^{NaCN} = 8.8 \pm 0.3$ mM NaCN) and k_{on}, resulting in an approximate dissociation rate constant ($k_{off} \approx 2.3 \pm 0.1$ s^{-1}).

Similarly, fitting the stopped-flow traces for NaCN binding to **ES** with a single exponential function resulted in a poor fit of the data, while very good fits were obtained with double exponential fitting (Figure 5B, residuals), again agreeing with the EPR data above, which show one high-spin and one low-spin species. Plotting the observed rates from the double exponential fitting versus NaCN concentration (Figure S7D) resulted in two linear plots with negative or near zero y-intercepts, where the slopes of the two fitttings may correspond to NaCN binding to the high-spin and low-spin species ($k_{on}(1) = 0.0163$ mM^{-1} s^{-1}, and $k_{on}(2) = 0.0096$ mM^{-1} s^{-1}). The negative or near zero y-intercepts suggest that the dissociation rate (k_{off}) is small. Fitting the data to just a single exponential equation resulted in a plot (Figure S7E) for the $1/\tau_1$, NaCN concentration dependence that was again linear with a small negative y-intercept. The slope from this plot gives an approximate rate for NaCN binding to **ES** ($k_{on} \approx 0.014$ mM^{-1} s^{-1}). One can then estimate the dissociation rate constant based on the measured K_D value ($K_D^{NaCN} = 0.083 \pm 0.006$ mM) and k_{on}, resulting in an approximate dissociation rate constant ($k_{off} \approx 0.0012 \pm 0.0001$ s^{-1}). In order for cyanide to have a 100-fold higher affinity ($K_D = k_{off}/k_{on}$) for **ES** over the **E**, as seen in the titration experiments, yet have an apparent ~19-fold slower cyanide binding rate (k_{on}), as seen in the stopped-flow experiments, the cyanide dissociation rate (k_{off}) would need to be, and indeed is, ~1900-fold slower from **ES**CN as compared to **E**CN, suggesting that the **ES**CN species is much more stable than the **E**CN species. In these cyanide binding studies, a triple exponential equation was required to adequately fit the kinetic traces for cyanide binding to the **E**, while only a double exponential equation was necessary to fit the data for cyanide binding to **ES**. This difference suggests that substrate binding may eliminate one of the heme states and possibly slow or perturb the equilibrium between the different high-spin and low-spin states observed by EPR spectroscopy.

pH Dependence of K_D Values for NaCN Binding. As multiple high- and low-spin Fe(III) species are observed for CYP121 in dynamic equilibrium as a function of pH, NaCN was again used as a probe to examine the effects of pH on ligand binding/exchange to both **E** and **ES**, by measuring the K_D value for NaCN at different pH values ranging from 7.5 to 10.4 (Figure 6). Lower pH values were not examined due to the evolution of toxic hydrogen cyanide gas under acidic

DOI: 10.1021/jacs.7b08911
J. Am. Chem. Soc. 2017, 139, 17484–17499

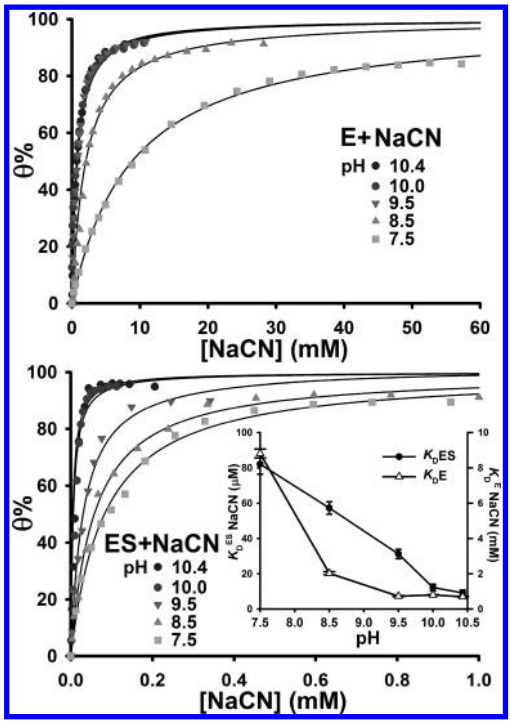

Figure 6. Comparison of NaCN binding curves for NaCN binding to **E** (top) and to **ES** (bottom), showing the calculated percent fraction bound (θ%). Binding of NaCN was monitored by titrating a 10 μM solution of CYP121 with NaCN and monitoring the absorbance until equilibrium was established after each successive addition of NaCN. The titration of the NaCN binding was monitored at 408 and 394 nm for **E** and **ES**, respectively. At pH 7.5, 8.5, and 9.5, cYY (465 μM) was added to 10 μM heme. cYY (1.3 mM) was used for titrations performed at pH 10.0 and 10.4, due to the higher K_D for cYY at high pH conditions. (Inset) pH dependence of K_D^{NaCN} values from NaCN titration experiments for cyanide binding to the **E** and **ES**.

conditions. **ES** binds cyanide with a higher affinity than **E** at every pH (Figure 6, inset), consistent with the results obtained from the stopped-flow study, while the K_D value for NaCN binding to **ES** steadily decreases from pH 7.5 to 10.4. The affinity of **E** for cyanide drastically drops from pH 7.5 to 8.5, from 8.8 ± 0.2 mM to 2.0 ± 0.1 mM NaCN (0.75-fold decrease), while the K_D value for NaCN binding to **ES** only decreases by 0.3-fold decrease between pH 7.5 and 8.5. This change in affinity for cyanide between pH 7.5 and 8.5 corresponds to the maximum yield of ls-**E**2 observed in EPR samples at pH 8.5 (Figure 1B).

Determination of the pK_a of cYY. In the crystal structure of **ES**, the proximal tyrosine closely approaches the heme center and is involved in a short H-bonding network with the axial water and a second water in the active site,[14] discussed further below. As the pK_a of the phenol group of tyrosine is around 10.1.[38] The protonation state of the substrate, cYY, is likely to affect the axial ligand, cyanide binding, and metal spin-state.

The pK_a of cYY was obtained by collecting UV−vis spectra of cYY in buffered solutions ranging from pH 6.0 to 12.5 (Figure 7). At low pH, the neutral-protonated (cYY-OH) has an absorbance band at 275 nm ($\varepsilon_{275\ nm}$ = 3150 ± 30 M^{-1} cm^{-1}). While under basic conditions a new chromophore for the monoanionic substrate (cYY-O^-) is observed at 292 nm ($\varepsilon_{292\ nm}$ = 5450 ± 35 M^{-1} cm^{-1}). By following the change in absorbance at 292 nm as a function of pH, the pK_a of cYY (pK_a = 9.90 ± 0.02) could be determined (Figure 7, inset). In EPR experiments the g = 8 signal from the hs-**ES** was observed to shift as the pH increased to 10.4 (Figure 1D), likely due to binding of the anionic substrate in the active site.

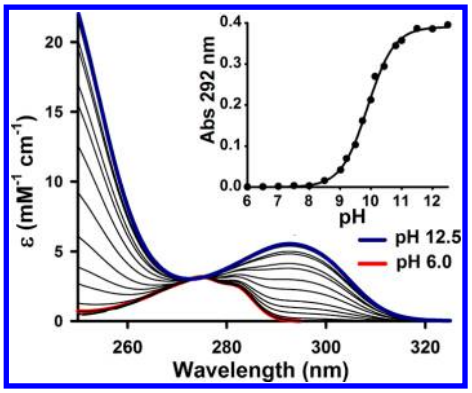

Figure 7. UV−vis spectra of cYY (150 mM) at pH 6.0−12.5 (pH-independent isosbestic point, $\varepsilon_{275\ nm}$ = 3150 ± 30 M^{-1} cm^{-1}). The inset shows the formation of monoanionic cYY monitored at 292 nm as a function of pH, and data fitted to pK_a = 9.90 ± 0.02. The monoanionic substrate (cYY-O^-) has an absorbance band in the near UV at 292 nm ($\varepsilon_{292\ nm}$ = 5450 ± 35 M^{-1} cm^{-1}).

pH Dependence of the K_D^{cYY}. The effect of the protonation state of cYY on substrate binding affinity was studied by measuring the dissociation constant (K_D) for **ES** in buffers ranging from pH 6 to 10.4 (Figure 8). Representative titration spectra and difference spectra can be found in Figure S8. Between pH 6.0 and 8.5, the K_D for cYY was ~23 μM, similar to what was previously reported (19.4 ± 0.6 μM cYY, pH 7.2).[20] Above pH 8.5, the K_D value increases, and at pH 10.4, the K_D has increased ~7-fold to 158 ± 6 μM. The increasing K_D suggests that the enzyme has a lower affinity for the monoanionic substrate and that the phenol group of cYY is likely involved in H-bond interactions with the enzyme which stabilize the **ES** complex, where it specifically acts as an H-bond donor.

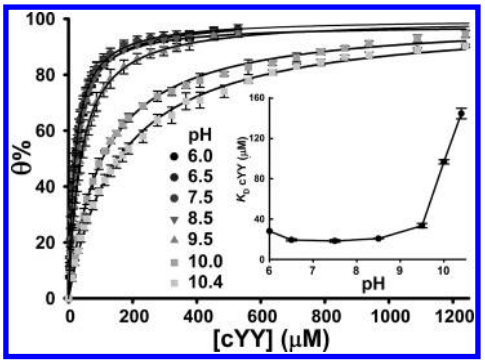

Figure 8. pH dependence of cYY binding to **E**. Titrations were performed in triplicate at pH 6.0, 6.5, 7.5, 8.5, 9.5, and 10.4. Titrations were monitored by following the amplitude difference between 386 and 419 nm over the course of the titration and fitted with one site saturation curve. Data are displayed as percent fraction bound (θ%). The inset shows K_D^{cYY} pH dependence from cYY titration experiments. K_D^{cYY} values at pH 7.5 and 10.4 are 19.4 ± 0.6 and 158 ± 6 μM cYY, respectively.

Whereas the affinity of the primary substrate cYY decreases at high pH (Figure 8, inset), the affinity of the secondary substrate analogue, NaCN, for **ES** increases with pH (Figure 8,

DOI: 10.1021/jacs.7b08911
J. Am. Chem. Soc. 2017, 139, 17484−17499

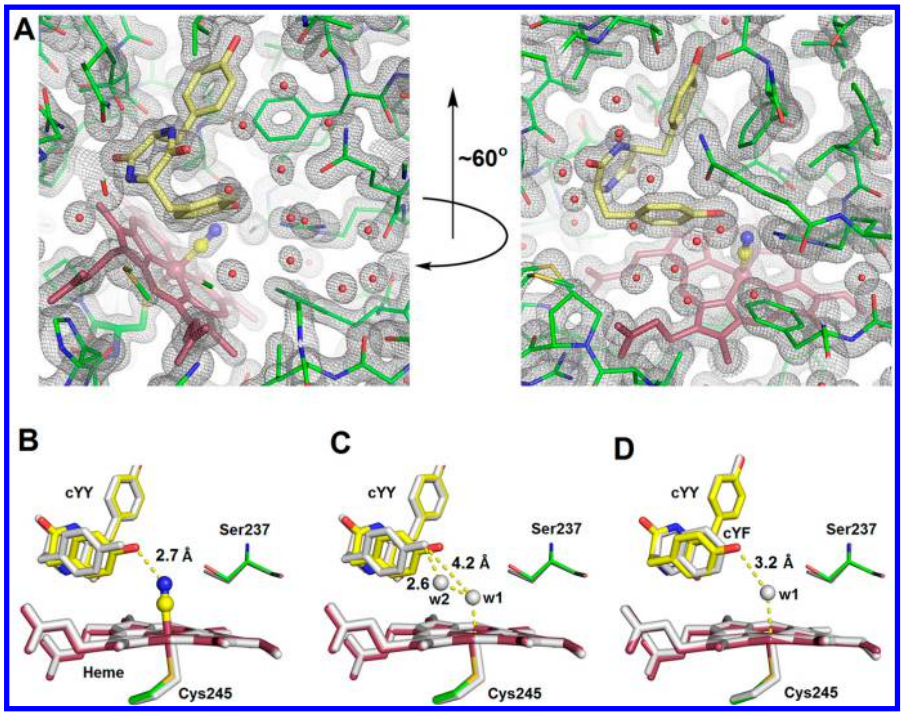

Figure 9. (A) Electron density map of the active site of the **ES**CN (PDB entry 5WP2, 1.4 Å) crystal structure, cYY highlighted in yellow and heme shown in dark raspberry. The $2F_o - F_c$ density (mesh) is contoured at the 1 σ level. (B,C) Overlays of **ES**CN (colored) with **ES** (PDB entry 3G5H, 1.4 Å; gray). The two ordered water molecules belong to the **ES** structure. Panel C shows the H-bonded water network of **ES**. (D) Overlay of the enzyme−cYF complex (PDB entry 4IQ9, 1.8 Å; gray) with the active site of the **ES**CN. The ordered water molecule belongs to the **E**-cYF structure.

inset). Taken together, these observations suggest that either the monoanionic substrate can stabilize the cyanide adduct, or the protonation state of cyanide (pK_a 9.3) results in an additional equilibrium between hydrogen cyanide and the cyanide anion, where the cyanide anion would be expected to bind stronger to the ferric heme, competing better the aqua or hydroxide ligand.

pH Dependence of UV−Vis Spectrum of E and ES. The dependence of the UV−vis spectra of **E** on pH was determined over the range of 6.5 to 10.4 (Figure S9). Subtle spectroscopic changes were observed during the titration of the **E** from pH 6.5 to 9.5 (Figure S9A,B), this is best seen as a shift in the Soret band from 395 to 430 nm observed in the difference spectrum, consistent with the conversion between ls-**E**1 and ls-**E**2 species observed over the same pH range by EPR (Figure 1). Increasing the pH of the solution from pH 9.5 to 10 (Figure S9C,D), resulted in an increase in the absorbance bands at 422 nm with concurrent decrease in the Soret shoulder at 390 nm with additional spectral changes in the visible region. These spectroscopic changes are also consistent with the increase in the hs-**E**1 observed by EPR between pH 9.5 and 10.0. Further increasing the pH from 10.0 to 10.4 (Figure S9E,F) resulted in spectral changes nearly opposite that observed between pH 9.5 and 10.0, as seen by a decrease in the bands at 390 nm, but with a smaller amplitude increase in the shoulder at 425 nm. Again these spectral changes are consistent with the EPR data, which showed a decrease in the ls-**E**2 signal with increasing yield of hs-**E**2 and a shift in the high-spin signal from g = 8.01 (hs-**E**1) to 7.99 (hs-**E**2). The spectroscopic changes between the different high-spin and low-spin species could be followed by monitoring the titration at 390 or 425 nm over the course of the titration (Figure S10). The titration curve clearly shows three different sigmoidal traces between pH 6.5 and 10.4. Because of the limited pH range of the experiment, the small amplitude of the observed spectral changes, and the overlap of the chromophores for the different species, it is difficult to rigorously determine the pK_a values for the conversion between the different observed species by UV−vis and EPR, though apparent pK_a values of ∼7.5, ∼9.6, and >10.3 can be estimated.

The pH titration of the **ES** was also performed by UV−vis (Figure S11). In these experiments, an increase in absorbance was observed in the UV range due to the deprotonation of the cYY substrate (Figure 7). Only a small increase in Soret band is observed at 418 nm at high pH, due to the lower affinity of CYP121 for cYY (Figure 8). This again is consistent with the EPR pH-dependent data in which only a very subtle shift in the g values was observed between pH 6.5 and 10.4, as well as little change in the ratio of hs- to ls-**ES**.

X-ray Crystal Structure of [Fe(III)-CYP121(cYY)CN]. To obtain crystals of CYP121 it was necessary to first remove the N-terminal His-tag using thrombin protease. Crystals of **ES** were prepared by crystallizing CYP121 in the presence of cYY. The crystal of the ternary **ES**CN complex was obtained by soaking crystals of **ES** in 50 mM NaCN at pH 8 for 2 h (Figure 9, PDB entry 5WP2). Despite an extensive effort we were unable to obtain a crystal structure of the **E**CN complex likely because of to the lower affinity of the cyanide ligand to **E**. The **ES**CN crystals were found to belong to space group $P6_522$ (Table 3), as previously observed for crystals of the enzyme and enzyme−substrate complexes.[14] The structure was solved by molecular replacement and refined to 1.44 Å. The $2F_o - F_c$ density map of the **ES**CN complex (Figure 9A) clearly shows the density for both the cYY substrate bound in the active site and the cyanide coordinating in a nearly linear, end-on binding mode to the six-coordinate iron. The heme prosthetic group has two distinct conformations related by a 180° flip in the ligand-free structure.[19] After substrate binding, the heme group

DOI: 10.1021/jacs.7b08911
J. Am. Chem. Soc. 2017, 139, 17484−17499

Table 3. Crystallization Data Collection and Refinement Statistics

data collection	CYP121 + CN^- + cYY
wavelength (Å)	1.0
resolution	50.00−1.44 (1.49−1.44)[a]
space group	$P6_522$
cell dimensions	
a, *b*, *c* (Å)	77.9, 77.9, 263.6
α, *β*, *γ* (deg)	90, 90, 120
total reflections	1 690 455
unique reflections	86 668
multiplicity	19.5 (17.2)[a]
completeness (%)	100.0 (99.9)[a]
mean $I/\sigma(I)$	33.18 (2.19)[a]
Wilson *B*-factor	18.12
R_{merge}[b] (%)	10.5 (96.1)[a]
refinement	
resolution	22.58−1.44
no. reflections, refinement	86 485
no. reflections, *R*-free	4338
R_{work}[c]/R_{free}[d] (%)	17.94/19.49
no. of atoms/*B*-factors (Å^2)	3867/23.06
protein	3140/21.30
heme	73/16.61
CYY	42/16.86
CN^-	2/14.09
SO_4^{2-}	20/34.77
water	590/33.30
root-mean-square deviation	
bond lengths (Å)	0.007
bond angles (deg)	0.906
Ramachandran statistics	
favored (%)	99.49
allowed (%)	0.51
outliers (%)	0.00
PDB entry	5WP2

[a]The values in parentheses are for the highest resolution shell. [b]$R_{merge} = \sum_i|I_{hkl,i} - \langle I_{hkl}\rangle|/\sum_{hkl}\sum I_{hkl,i}$, where $I_{hkl,i}$ is the observed intensity, and $\langle I_{hkl}\rangle$ is the average intensity of multiple measurements [c]$R_{work} = \sum||F_o| - |F_c||/\sum|F_o|$, where $|F_o|$ is the observed structure factor amplitude, and $|F_c|$ is the calculated structure factor amplitude. [d]R_{free} is the *R*-factor based on 5% of the data excluded from refinement.

has only one conformation.[14] In our **ESCN** complex structure, the heme center presents in one conformation.

A 2.0 Å Fe−C bond distance was observed with a nearly linear Fe−C−N geometry of 175°. Ser237, an active site residue in the heme distal pocket, is perturbed due to the presence of the bound CN^- ligand. It rotates by ∼20° away from the CN^- binding site (Figure 9), presumably due to steric clashing from the nitrogen atom. The overall position of other residues lining the substrate binding pocket were unaffected by CN^- binding when compared to the previously published binary **ES** complex (Figure 9A).[14] A side-by-side comparison of the **ES** and **ESCN** complex structures is shown in Figure S12. The RMSD value for the comparison of the active site within 5 Å around the heme center of **ES** and **ESCN** structures is 0.1 Å. While the position of the distal tyrosine of the substrate was unaffected by cyanide binding, the binding geometry of the proximal tyrosine was significantly affected, which was observed to move by 1.0 Å toward the cyanide ligand. The binding of cyanide to the metal positions the substrate closer to the heme for subsequent oxidation during catalysis (Figure 9B) and results in the displacement of both the axial water ligand and the second sphere water from the active site. The cause for these observed changes are likely due to the loss of a short hydrogen-bonding network from the proximal tyrosine to the iron bound water. This network involves two ordered water molecules, w1 and w2 (Figure 9C), which are observed in several published CYP121 substrate−complex crystal structures (PDB entries 3G5H, 1N4G, 4IQ9, 4IPW, and 5IBI).[14,19,20,39]

Characterization of CYP121, E, ES, ECN, and ESCN Complexes by ^{1}H ENDOR Spectroscopy. To analyze the chemical nature of the solvent-derived ligand and the active-site water network, both **E** and **ES** were characterized by ^{1}H ENDOR spectroscopy. Here, we will designate the three *g*-tensor values observed in the EPR spectrum of each species as g_z, g_y, and g_x, for the *g* values observed for each species from low to high magnetic field. The three *g* values correspond to the three orthogonal axes of the complex, where for low-spin heme proteins the unique g_z axis ($g \approx 2.4$) is thought to lie nearly perpendicular to the plane of the heme.[40] ^{1}H ENDOR spectra collected at the magnetic field corresponding to g_z will reveal signals from the enzymes in the sample in which the g_z axis of the heme is oriented along the magnetic field of the spectrophotometer and report structural information for nuclei along this axis. This orientation dependence gives structural information between the unpaired electron residing mainly in an atomic orbital of the metal (or molecular orbitals including the heme and Fe ligands) and nuclei in the active site of the enzyme. The magnitude of the nuclear hyperfine coupling relates to the distance between the ^{1}H from the paramagnetic center or electronic structure of the radical species. Detailed spatial information can thus be obtained from a rigorous analysis of the EPR and ENDOR data.[40−43]

Concentrated CYP121 samples with ≥1 mM heme were prepared for ENDOR analyses by slowly submerging CYP121 samples in liquid nitrogen to maximize the yield of the low-spin species. The ^{1}H ENDOR spectrum of **E** at pH 7.5, at *g* values corresponding to the ls-**E1**, are shown in Figure S13. The continuous-wave ENDOR spectrum acquired at the low-field component (g_z) shows a broad absorbance features at $\nu_H \pm 4$ MHz centered around the ^{1}H Larmor frequency. This signal likely originates from the strongly coupled axial solvent ligand bound to the ferric heme.[40−43] Another well-resolved signal is observed for the spectrum acquired at g_y, which has a sharp peak at 2.5 MHz with a weaker feature at −2.5 MHz. The spectrum acquired at g_y also has distinguishable shoulders at ν_H ±1 MHz and signals from several weakly coupled protons with *A* values less than 1.4 MHz.

Figure 10 shows overlays of the spectra for **E** and **ES** collected at the magnetic fields corresponding to their respective g_z and g_y. The ^{1}H ENDOR signals have been normalized by their signal intensity for better comparison. Again the ^{1}H ENDOR spectrum of ls-**E**1 (pH 7.5) shows multiple doublets from protons near the low-spin ferric center, with *A* values of ∼8, 5, and 2 MHz.[43] Spectra of **ES** at pH 7.5 show a new doublet at $\nu_H = \pm 1.3$ MHz (A = 2.6 MHz, g_z) corresponding to the ls-**ES**1. This signal is not observed for the ls-**ES**2 complex prepared at pH 10.4, suggesting that the 2.6 MHz signal may originate from the phenol proton (pK_a = 9.90 ± 0.02) of the cYY, which is involved in a hydrogen-bonding interaction with the axial solvent molecule. At pH 10.4, the sharp feature at $\nu_H = \pm 2.5$ MHz observed for **E** and **ES** at pH 7.5 is also perturbed and splits into two peaks with *A* values of 4.4 and 5 MHz. This splitting may result from the

DOI: 10.1021/jacs.7b08911
J. Am. Chem. Soc. 2017, 139, 17484−17499

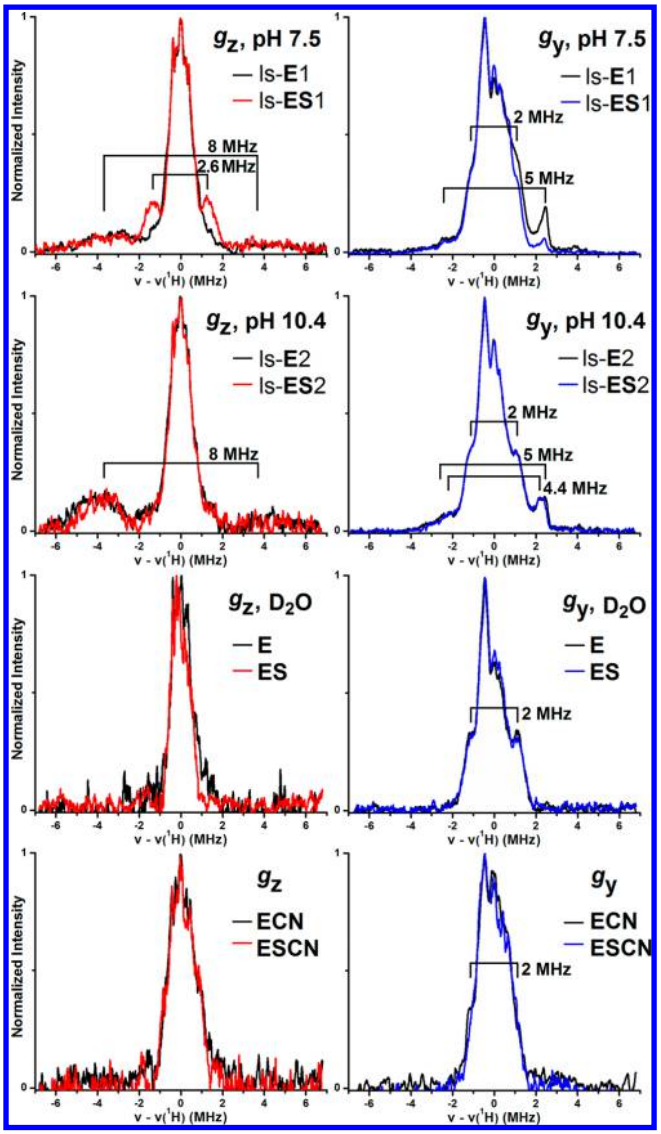

Figure 10. ENDOR spectra of **E** and **ES**. Samples prepared (top to bottom) at pH 7.5 (ls-**E**1), at pH 10.4 (ls-**E**2), or in D_2O (pD 7.5), and in complex with cyanide (**E**CN and **ES**CN). ENDOR spectra shown were acquired at magnetic fields corresponding to g_z (low-field feature, left) and g_y (midpoint of derivative-shaped feature, right). Samples contained 1.0 to 1.7 mM CYP121 heme concentration; **ES** and **ES**CN were prepared with 1.3 mM cYY, and **E**CN and **ES**CN with 55 mM NaCN. The spectra have been normalized and centered at ^{1}H Larmor frequency for each magnetic field for comparison. Spectrometer conditions can be found in Materials and Methods.

deprotonation of the substrate and/or the axial water at high pH, which should affect the H-bonding network between the axial solvent ligand (aqua/hydroxide), cYY (phenol/phenolate), and the second sphere water, as observed in the crystal structure of **ES** (Figure 10C).

To aid in the assignment of the different signals observed in the ^{1}H ENDOR spectrum and to assign solvent-exchangeable protons, the spectra of **E** and **ES** were also acquired for samples prepared in D_2O (pD = 7.5). In these samples the overall intensity of the spectrum decreased for the weakly coupled protons (Figure S12). The signals assigned above to the axial aqua/hydroxide (ν_H = ±4 MHz), the second sphere water (ν_H = ±2.5 MHz), and the cYY phenol proton (ν_H = ±1.3 MHz) are not observed in D_2O, consistent with these assignments (Figure 10). The signals for the ν_H = ±1 MHz (g_y) doublet becomes better resolved for the samples prepared in D_2O. In previous ^{1}H ENDOR studies of cytochrome P450's, these non-solvent-exchangeable protons have been assigned to the β-^{1}H of the axial cysteine ligand or to protons on the porphyrin ring.[40,43]

The ^{1}H ENDOR spectrum of **E**CN and **ES**CN resembles that of the samples prepared in D_2O, where the signals assigned to the axial water/hydroxide (ν_H = ±4 MHz) and the second sphere water (±2.5 MHz) are absent, consistent with the crystal structure of **ES**CN (Figure 9B), which shows the displacement of both the axial water molecule and the second sphere water upon cyanide binding to the **ES** complex. It should be noted that the 2.6 MHz proton from cYY is not seen in the **ES**CN complex g_z spectrum. A plausible explanation is that a disruption of the H-bonding network with the cYY may result in a disruption of the orientation of the phenol protons.

DISCUSSION

Dynamic Equilibrium. In EPR studies of the **E**, we observed two low-spin (ls-**E**1 and ls-**E**2) and one high-spin (hs-**E**1) species in equilibrium with each other, at pH 7.5.[15] The two low-spin species are hexacoordinate heme centers, and the high-spin species is likely a pentacoordinate heme, in which the axial solvent-derived ligand has been displaced. In the pH-dependent EPR experiments, the two low-spin species appeared to be an acid/base pair with a pK_a near 7.5 (Scheme 3). Possible sites for this acid/base group include the proximal cysteine thiol/thiolate ligand or the axial aqua/hydroxide ligand. The protonation state of the axial cysteine ligand was previously investigated for CYP121 by Dunford et al.[28] They found that the as-isolated Fe(III)-CYP121 contained a thiolate ligand with a pK_a less than 6.5. Further, they were able to determine the pK_a of the thiol/thiolate transition of 7.2 ± 0.1 upon carbon monoxide binding. The protonation state of the cysteine ligand was also probed by ^{1}H ENDOR in this work. Spectra of the **E**CN and **ES**CN complexes acquired at pH 7.5 (Figure 10) were found to be comparable to the spectra of the **E** and **ES** complexes in D_2O, with the absence of any strongly coupled protons. This similarity suggests not only that the axial solvent-derived ligand has been displaced by CN^-, but also that the cysteine ligand (Cys345) of the **E**CN and **ES**CN complexes remains unprotonated in the ferric-cyanide complexes (pK_a < 7.5). The protonation state of the thiolate ligand is very important for the P450 chemistry (Scheme 2), and this has been well-characterized previously in other P450 enzymes.[44−46]

Previous spectroscopic studies of Fe(III)-P450s, from the thermoacidophilic crenarchaeon *Sulfolobus tokodaii*, observed a similar acid−alkaline transition with a pK_a of 8.7 due to an equilibrium between the aqua/hydroxide species for the axial ligand. At pH 7, only one low-spin species with g values of 2.42, 2.25, and 1.92 was observed while at pH 10 the formation of a second more rhombic low-spin species with g values of 2.49, 2.24, and 1.91 was reported.[47] Likewise, the two low-spin species ls-**E**1 and ls-**E**2 observed in our EPR with CYP121 may be assigned to the aqua and hydroxide adducts (Scheme 3), respectively, with a pK_a of ~7.5. Above pH 8.5, the ls-**E**2 signal is observed to convert to a second high-spin species (hs-**E**2). This pH effect may be due to structural changes, under basic conditions that favor the five-coordinate heme. Alternately, the hs-**E**2 species may originate from a six-coordinate heme with a hydroxide ligand. As the hydroxide anion is a strong π-base with two lone pairs of π-symmetry, the high-spin species could

DOI: 10.1021/jacs.7b08911
J. Am. Chem. Soc. 2017, 139, 17484−17499

Scheme 3. Diagram of Probable Equilibria among E, ES*, ES, and Cyanide Adducts ECN and ESCN[a]

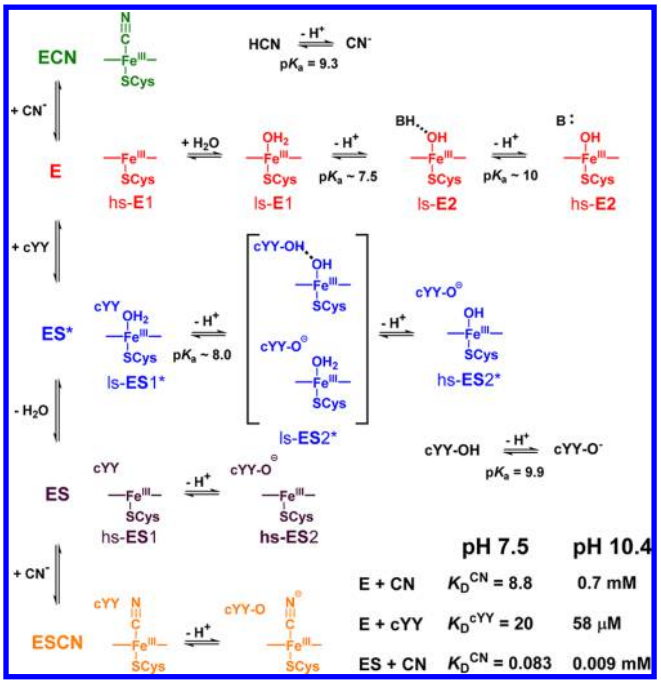

[a]An apparent equilibrium exists between two low-spin (ls-**E**1, ls-**E**2), and one high-spin (hs-**E**1) form of the enzyme at pH 7.5, in which ls-**E**1 and ls-**E**2 likely have either an aqua or hydroxide axial ligand, respectively. The hs-**E**1 is a probably five-coordinate Fe(III)-heme. A similar equilibrium exists between multiple low-spin (**ES***) and high-spin (**ES**) species to which the substrate cYY (pK_a = 9.9) can be bound in either the neutral or anionic form. Ligand exchange likely proceeds through a dissociative mechanism where the cyanide (pK_a = 9.3) binds as an anionic ligand to the five-coordinate hs-**E** or hs-**ES** centers. cYY binding in the active site appears to slow the rate of cyanide binding, but stabilize the **ES**CN adduct over the **E**CN adduct (Table 3).

originate from a change in the H-bonding network to the axial hydroxide ligand under basic conditions. This could result in an increase in the π-basicity of the hydroxide ligand, a lower ligand field, and a conversion from a low-spin Fe(III)-OH to a high-spin Fe(III)-OH species (Scheme 3).

The low- and high-spin EPR signals of **ES** are also both sensitive to changes in pH, showing subtle changes in the g values upon increasing the pH (Figure 1 and Table 1). This observation suggests an equilibrium between two low-spin (ls-**ES**1 and ls-**ES**2) and two high-spin species (hs-**ES**1 and hs-**ES**2). The two low-spin species may again be due to different forms of the **ES** complex with either an aqua or hydroxide ligand (Scheme 3). Another possible explanation for multiple low- and high-spin **ES** species could originate from the binding of either the neutral or monoanionic cYY (pK_a = 9.9, Figure 7) in the active-site. The protonation state of the phenol group of cYY is likely to affect the observed hydrogen-bonding network between the axial solvent-derived ligand and cYY, or result in other subtle structural changes affecting the electronic structure. A similar effect may explain the observed increase in the yield of hs-**E** with pH, due to the deprotonation of the second sphere amino acid residue Ser237, which is within H-bonding distance (O−O, 2.85 Å) of the axial solvent-derived ligand (PDB 3G5F).[14] The protonation state of the substrate may also affect the binding of diatomic ligand, cyanide, O_2, and (hydro)peroxo species generated during catalysis (Scheme 2). Indeed, under basic conditions, cyanide was observed to have a significantly higher affinity for **ES** (Figure 6 and Table 4). The protonation state and pK_a of cYY could also affect catalysis, as the oxidation of cYY has been proposed to proceed through hydrogen atom abstraction from the phenol group by either a peroxo species or by Compound I [Fe(IV)-oxo(heme radical cation)].[14,15,48]

Additional complexity is observed for CYP121 in EPR experiments, in which EPR samples that were frozen by rapidly submerging in liquid ethane showed significantly larger populations of high-spin ferric heme (Figure 2), suggesting a dynamic equilibrium between the five-coordinate, high-spin and six-coordinate, low-spin species for both **E** and **ES**. The observed higher population of hs-**ES** observed in these samples is also more consistent with the UV−vis spectrum of **ES**, which is characteristic of a high population of high-spin heme.[17] This temperature dependence was also observed by UV−vis spectroscopy for **E**, which exhibited spectral changes consistent with a conversion of a portion of the low-spin to high-spin heme as the temperature was lowered from 30 to 4 °C. Similar thermodynamic equilibria between the high- and low-spin hemes have been observed for different P450 isoforms.[17,32]

A clue to this dynamic equilibrium was previously observed by us in stopped-flow experiments monitoring cYY binding to CYP121 at pH 7.5.[15] The kinetics suggested a two-step mechanism for cYY binding to form an initial enzyme−substrate complex denoted **ES*** (Scheme 3), which then

Table 4. Comparison of k_{on}, k_{off}, and K_D Values for Cyanide Binding to P450 Enzyme and Enzyme−Substrate Complexes

P450 enzyme complex[a]		k_{on} (mM^{-1} s^{-1})	k_{off} (s^{-1})	K_D^{NaCN} (mM)	refs
Fe(III)-CYP121, **E**	pH 7.5	0.26	2.3 ± 0.1	8.8 ± 0.3	this work
	pH 10.4			0.70 ± 0.02	this work
[Fe(III)-CYP121(cYY)], **ES**	pH 7.5	0.014	0.0012 ± 0.0001	0.083 ± 0.006	this work
	pH 10.4			0.0092 ± 0.0016	this work
CYP3A4		10	4	0.4	35
[CYP3A4(T)]		0.13	0.18	1.4	35
Fe(III)-eNOS		1.8	22	12	36
[Fe(III)-eNOS(Arg)]		0.005	0.2	40	36
Fe(III)-CYP101				0.12	34
[Fe(III)-CYP101(cam)]				4.7	34

[a]T = testosterone, cam = camphor, Arg = arginine, cYY = cyclodityrosine.

DOI: 10.1021/jacs.7b08911
J. Am. Chem. Soc. 2017, 139, 17484−17499

equilibrated with a second enzyme−substrate complex. Based on the observed rate constants, one can simulate the time course for the formation of the **ES** complexes and the final equilibrium concentrations of the **E**, **ES***, and **ES** (Figure S14). These simulations have helped to gain a better understanding of **ES***. At 700 μM cYY, **ES*** is predicted to form in the first 60 ms to a 73% yield. Equilibration between **ES*** and **ES** is then relatively slow, taking ∼1 s. Under these conditions, at equilibrium, the expected concentration of the three enzyme-species is expected to be 4% **E**, 42% **ES***, and 54% **ES**. This simulation is consistent with the ratio of high-spin and low-spin species observed in the EPR samples frozen rapidly in liquid ethane, where a significant population of both hs-**ES** and ls-**ES** are observed. The initial cYY adduct **ES*** is likely a low-spin six-coordinate heme center prior to dissociation of the axial, solvent-derived ligand (Scheme 3), which then forms (equilibrates with) a high-spin form of the **ES** complex upon dissociation of the axial solvent ligand.

Ligand Exchange: Cyanide Binding. Though cyanide is not a perfect substrate analogue for O_2 (or H_2O_2) binding due to its preferred linear, end-on binding mode, it can still give general information on the mechanism of substrate binding. In particular, the cyanide binding experiments can help study the mechanism and kinetics of metal−ligand exchange and probe the effects of the primary organic substrate, cYY, on metal−ligand exchange, thus giving insights into O_2 binding, activation, and catalysis.

Binding of the anionic π-acid NaCN ligand to **E** or **ES** results in UV−vis and EPR spectroscopic changes consistent with the formation of low-spin [Fe(III)-CYP121(CN)] and [Fe-(III)-CYP121(cYY)CN] complexes.[34−36] Titration experiments allowed us to obtain K_D values for NaCN binding to **E** and **ES**, respectively (Table 4). The affinity for cyanide binding to **ES**, at pH 7.5, is 100-fold higher than for **E**. This increased affinity upon substrate binding is consistent with a stepwise binding mechanism (Scheme 2), where substrate binding in the active site of the enzyme would precede and potentially facilitate Fe-reduction by altering the redox potential before O_2 activation or H_2O_2 peroxide binding in the peroxide shunt pathway,[16] thus protecting the enzyme from activating O_2 in the absence of substrate and conserving reducing equivalents supplied by a reductase.

The NaCN transient kinetic binding studies show complex binding kinetics, likely due to the presence of multiple high- and low-spin species observed by EPR in equilibrium with each other. Interestingly, though **ES** exhibits a 100-fold higher affinity for cyanide, the actual second-order rate constant for cyanide binding was ca. 19-fold lower to **ES** than to **E**. The faster binding to **E** is consistent with a more open active site for **E** than **ES**, where the substrate provides some steric constraints for cyanide binding. Access of the exogenous cyanide ligand to the heme center is less favorable to **ES** than to **E** but results in a stronger Fe-CN bond in **ES**CN than in **E**CN.

Comparison of the observed kinetic constants (Table 4) for cyanide binding to other P450 enzyme and enzyme−substrate complexes shows several trends: (1) the second-order rate constant (k_{on}) is higher for cyanide binding to the **E** than to the **ES** complexes; (2) the cyanide dissociation constant (k_{off}) is higher for the **E** than the **ES** complexes; and (3) cyanide binds to the **ES** complex significantly weaker (3−40-fold higher K_D) than to the enzyme alone for CYP3A4, CYP101, and eNOS. The third trend was found to be the opposite for cyanide binding to CYP121 where the enzyme−substrate complex displays a 100-fold higher affinity for cyanide then to the free enzyme. This shows cYY plays an additional role in stabilizing the ternary **ES**CN species as compared to other P450s.

Hydrogen-Bonding Network at the Distal Heme Pocket. Cyanide binding to **ES**, though slower than to **E**, must result in interactions which form a significantly more stable adduct. Comparison of the crystal structures of **E** (PDB entry 1N40, 1.06 Å), binary complex **ES** (PDB 3G5H, 1.4 Å), and ternary complex **ES**CN (PDB 5WP2, 1.4 Å) is consistent with these observations, where the active site of **E** is more open, with several waters occupying the active site, versus **ES**, where we observe a short hydrogen-bonding network between the two remaining water molecules in the active site, connecting the axial solvent ligand and the proximal phenol group of cYY. Our ^{1}H ENDOR experiments also imply the presence of a hydrogen-bonding network between the axial water and the substrate (Figure 10). In **ES**CN, cyanide binding is observed to disrupt this hydrogen-bonding network, displacing the remaining two water molecules. O_2 or the proposed (hydro)-peroxo would be expected to bind in a bent end-on or side-on geometry occupying a similar space as these two waters and likely forming a similar hydrogen-bonding network with the substrate's phenol group. In this way, the cYY substrate may be playing a very important role in the initial binding and orientation of the O_2 adduct for subsequent O_2 activation and substrate oxidation.

The substrate-free structure exhibits a large active-site with a six-coordinate ferric ion and a solvent-derived axial ligand. The structure of the cYY-bound complex shows that cYY binds to the distal pocket of the heme with one of its tyrosine moieties adjacent to the Fe ion. A H-bond network is observed in the distal pocket of the heme center involving two ordered water molecules, w1 and w2 in Figure 9C, which are present in several published CYP121 ligand (substrate or analogue)-bound complex crystal structures (PDB entries 3G5H, 1N4G, 4IQ9, 4IPW, and 5IBI).[14,19,20,39] Besides 1N4G and 5IBI, the other the crystals all contain a substrate with an OH group positioned near the heme similar to the cYY-**ES** structure. The structure for 1N4G contains the small molecule 4-iodopyrazole which is bound far from the heme center, likely maintaining the integrity of the active site to resemble that of the enzyme only structure.[19] Conversely, a similar case can be made for the 5IBI structure, the phenol groups are all pointed away from the heme cofactor. Thus, the binding site near the heme is less crowded allowing for more water molecules to be present which can maintain a hydrogen bond network with w1 and w2. The other **ES** ligand-bound structures of CYP121 in the Protein Data Bank (PDB) contain small molecules that bind either distinctly compared to cYY or occupy the same space as one of the water molecules. The w1 molecule is bound directly to the Fe center and possesses a hydrogen bond to w2, 2.4 Å away. The w2 molecule in turn forms a H-bond to the phenol group of the proximal tyrosine moiety which is 2.6 Å away (Figure 9C). In the **ES** structure, this H-bond network is possibly involved in positioning the hydroxyl group of the proximal cYY near the heme.[14] Such a water-based H-bond network is found in both the enzyme-only structure and the binary complex but is missing in the ternary **ES**CN complex. The binding of CN, and possibly O_2, to **ES** apparently displaces the two waters from the active site, allowing for the reorientation of the proximal tyrosine, bringing it closer to the oxidizing species for reaction. Interestingly, it should be noted that in the previously published structure of CYP121 in

DOI: 10.1021/jacs.7b08911
J. Am. Chem. Soc. 2017, 139, 17484−17499

complex with cyclo-(L-tyrosine-L-phenylalanine) (**E**-cYF, PDB entry 4IQ9), the phenylalanine moiety was observed to be positioned toward the heme, and the second water involved in the H-bond network is not present (Figure 9D).[20] It is likely the more hydrophobic nature of the benzene ring compared to the phenol and the loss of a hydrogen bond to w2 are responsible for disruption of the network. In the **E**-cYF structure, the phenylalanine group is positioned closer to the heme center than the proximal tyrosine of cYY in the **ES** complex with cYY. In the previous study, it was also found that the cYF was first hydroxylated to cYY and then reacted further to form the cross-link and mycocyclosin.[20]

Concluding Remarks. Due to the great significance of CYP121 as a potential drug target for fighting TB infections, as well as general interest in the mechanism of this unique C−C bond coupling reaction performed by a P450 enzyme, we performed these kinetic, spectroscopic, and structural studies to probe the mechanism of metal−ligand exchange and investigate some unanswered questions from the initial structural characterization of the enzyme−substrate complex, in which UV−vis and EPR data appeared to be contradictory.[14] The work described above is aimed at reconciling the aforementioned discrepancies. It provides the first quantitative and qualitative atomic and molecular level study of this highly interesting enzyme that is significant both biomedically and from a basic science standpoint.

Our data show that cYY binding does indeed destabilize the solvent-derived ligand in solution at room temperature and that there is an apparent equilibrium between multiple low-spin and high-spin species in solution. Furthermore, binding of cYY results in stabilization of the bound diatomic ligand. Binding of the diatomic ligand O_2 results in a rearrangement of the active site, priming the substrates for efficient catalysis. The protonation state of the phenol group of cYY also affects the substrate affinity and the affinity for the CN^- ligand. Scheme 3 summarizes the observed equilibria among the different proposed species observed by UV−vis, EPR, and ENDOR and their relation to CN^- binding.

■ ASSOCIATED CONTENT

Supporting Information

The Supporting Information is available free of charge on the ACS Publications website at DOI: 10.1021/jacs.7b08911.

Figures S1−S14, providing spectroscopic characterization and K_D values for imidazole binding to CYP121, EPR temperature and microwave power saturation experiments, titration results, kinetic data, and structural comparisons (PDF)

■ AUTHOR INFORMATION

Corresponding Author

*Feradical@utsa.edu

ORCID

Aimin Liu: 0000-0002-4182-8176

Notes

The authors declare no competing financial interest.

■ ACKNOWLEDGMENTS

We thank Dr. Ralph T. Weber of Bruker BioSpin Corp for his advice in performing the ENDOR experiments and Dr. Inchul Shin for assistance in our attempts to obtain an ECN structure. This work was supported in whole or part by National Institutes of Health Grants GM108988 and GM107529 (to A.L.). L.M. acknowledges the Presidential Distinguished Research Fellowship of University of Texas at San Antonio. The single crystal X-ray synchrotron data were collected at the beamline 9-2 of SSRL beamline resource under the user program proposal 5B14. The SSRL user program is supported by the U.S. Department of Energy under Contract No. DE-AC02-76SF00515, and the SSRL Structural Molecular Biology Program is supported by the DOE Office of Biological and Environmental Research, and by the National Institutes of Health, National Institute of General Medical Sciences (P41GM103393).

■ REFERENCES

(1) Harland, C. W.; Rabuka, D.; Bertozzi, C. R.; Parthasarathy, R. *Biophys. J.* **2008**, *94*, 4718−4724.

(2) Sturgill-Koszycki, S.; Schlesinger, P. H.; Chakraborty, P.; Haddix, P. L.; Collins, H. L.; Fok, A. K.; Allen, R. D.; Gluck, S. L.; Heuser, J.; Russell, D. G. *Science* **1994**, *263*, 678−681.

(3) Keane, J.; Balcewicz-Sablinska, M. K.; Remold, H. G.; Chupp, G. L.; Meek, B. B.; Fenton, M. J.; Kornfeld, H. *Infect. Immun.* **1997**, *65*, 298−304.

(4) Silva Miranda, M.; Breiman, A.; Allain, S.; Deknuydt, F.; Altare, F. *Clin. Dev. Immunol.* **2012**, *2012*, 1−14.

(5) Golden, M. P.; Vikram, H. R. *Am. Fam. Physician* **2005**, *72*, 1761−1768.

(6) Centers for Disease Control and Prevention (CDC). Take-on-tuberculosis, https://www.cdc.gov/tb/publications/infographic/pdf/take-on-tuberculosis-infographic.pdf.

(7) Mak, A.; Thomas, A.; Del Granado, M.; Zaleskis, R.; Mouzafarova, N.; Menzies, D. *Am. J. Respir. Crit. Care Med.* **2008**, *178*, 306−312.

(8) Kliiman, K.; Altraja, A. *Ann. Intern. Med.* **2009**, *150*, 766−775.

(9) Kliiman, K.; Altraja, A. *Eur. Respir. J.* **2009**, *33*, 1085−1094.

(10) McLean, K. J.; Carroll, P.; Lewis, D. G.; Dunford, A. J.; Seward, H. E.; Neeli, R.; Cheesman, M. R.; Marsollier, L.; Douglas, P.; Smith, W. E.; Rosenkrands, I.; Cole, S. T.; Leys, D.; Parish, T.; Munro, A. W. *J. Biol. Chem.* **2008**, *283*, 33406−33416.

(11) Cole, S. T.; Brosch, R.; Parkhill, J.; Garnier, T.; Churcher, C.; Harris, D.; Gordon, S. V.; Eiglmeier, K.; Gas, S.; Barry, C. E., 3rd; Tekaia, F.; Badcock, K.; Basham, D.; Brown, D.; Chillingworth, T.; Connor, R.; Davies, R.; Devlin, K.; Feltwell, T.; Gentles, S.; Hamlin, N.; Holroyd, S.; Hornsby, T.; Jagels, K.; Krogh, A.; McLean, J.; Moule, S.; Murphy, L.; Oliver, K.; Osborne, J.; Quail, M. A.; Rajandream, M. A.; Rogers, J.; Rutter, S.; Seeger, K.; Skelton, J.; Squares, R.; Squares, S.; Sulston, J. E.; Taylor, K.; Whitehead, S.; Barrell, B. G. *Nature* **1998**, *393*, 537−544.

(12) Roback, P.; Beard, J.; Baumann, D.; Gille, C.; Henry, K.; Krohn, S.; Wiste, H.; Voskuil, M. I.; Rainville, C.; Rutherford, R. *Nucleic Acids Res.* **2007**, *35*, 5085−5095.

(13) Gondry, M.; Sauguet, L.; Belin, P.; Thai, R.; Amouroux, R.; Tellier, C.; Tuphile, K.; Jacquet, M.; Braud, S.; Courçon, M.; Masson, C.; Dubois, S.; Lautru, S.; Lecoq, A.; Hashimoto, S.-i.; Genet, R.; Pernodet, J.-L. *Nat. Chem. Biol.* **2009**, *5*, 414−420.

(14) Belin, P.; Le Du, M. H.; Fielding, A.; Lequin, O.; Jacquet, M.; Charbonnier, J.-B.; Lecoq, A.; Thai, R.; Courçon, M.; Masson, C.; Dugave, C.; Genet, R.; Pernodet, J.-L.; Gondry, M. *Proc. Natl. Acad. Sci. U. S. A.* **2009**, *106*, 7426−7431.

(15) Dornevil, K. D.; Davis, I.; Fielding, A. J.; Terrell, J. R.; Ma, L.; Liu, A. *J. Biol. Chem.* **2017**, *292*, 13645−13657.

(16) Denisov, I. G.; Makris, T. M.; Sligar, S. G.; Schlichting, I. *Chem. Rev.* **2005**, *105*, 2253−2277.

(17) Conner, K. P.; Schimpf, A. M.; Cruce, A. A.; McLean, K. J.; Munro, A. W.; Frank, D. J.; Krzyaniak, M. D.; Ortiz de Montellano, P.; Bowman, M. K.; Atkins, W. M. *Biochemistry* **2014**, *53*, 1428−1434.

DOI: 10.1021/jacs.7b08911
J. Am. Chem. Soc. 2017, 139, 17484−17499

(18) Luthra, A.; Denisov, I. G.; Sligar, S. G. *Arch. Biochem. Biophys.* **2011**, *507*, 26−35.
(19) Leys, D.; Mowat, C. G.; McLean, K. J.; Richmond, A.; Chapman, S. K.; Walkinshaw, M. D.; Munro, A. W. *J. Biol. Chem.* **2003**, *278*, 5141−5147.
(20) Fonvielle, M.; Le Du, M. H.; Lequin, O.; Lecoq, A.; Jacquet, M.; Thai, R.; Dubois, S.; Grach, G.; Gondry, M.; Belin, P. *J. Biol. Chem.* **2013**, *288*, 17347−17359.
(21) Bleaney, B.; Abragam, A. *Electron Paramagnetic Resonance of Transition Metal Ions*, 2nd ed.; Clarendon Press: Oxford, 1970.
(22) Otwinowski, Z.; Minor, W. *Methods Enzymol.* **1997**, *276*, 307−326.
(23) McCoy, A. J.; Grosse-Kunstleve, R. W.; Adams, P. D.; Winn, M. D.; Storoni, L. C.; Read, R. J. *J. Appl. Crystallogr.* **2007**, *40*, 658−674.
(24) Adams, P. D.; Afonine, P. V.; Bunkoczi, G.; Chen, V. B.; Davis, I. W.; Echols, N.; Headd, J. J.; Hung, L. W.; Kapral, G. J.; Grosse-Kunstleve, R. W.; McCoy, A. J.; Moriarty, N. W.; Oeffner, R.; Read, R. J.; Richardson, D. C.; Richardson, J. S.; Terwilliger, T. C.; Zwart, P. H. *Acta Crystallogr., Sect. D: Biol. Crystallogr.* **2010**, *66*, 213−221.
(25) Emsley, P.; Lohkamp, B.; Scott, W. G.; Cowtan, K. *Acta Crystallogr., Sect. D: Biol. Crystallogr.* **2010**, *66*, 486−501.
(26) ATSDR. *Toxicological profile for cyanide*; U.S. Department of Health and Human Services: Atlanta, GA, 2006.
(27) McLean, K. J.; Marshall, K. R.; Richmond, A.; Hunter, I. S.; Fowler, K.; Kieser, T.; Gurcha, S. S.; Besra, G. S.; Munro, A. W. *Microbiology* **2002**, *148*, 2937−2949.
(28) Dunford, A. J.; McLean, K. J.; Sabri, M.; Seward, H. E.; Heyes, D. J.; Scrutton, N. S.; Munro, A. W. *J. Biol. Chem.* **2007**, *282*, 24816−24824.
(29) Sligar, S. G. *Biochemistry* **1976**, *15*, 5399−5406.
(30) Fisher, M. T.; Sligar, S. G. *Biochemistry* **1987**, *26*, 4797−4803.
(31) Sharrock, M.; Münck, E.; Debrunner, P. G.; Marshall, V.; Lipscomb, J. D.; Gunsalus, I. C. *Biochemistry* **1973**, *12*, 258−265.
(32) Renaud, J. P.; Davydov, D. R.; Heirwegh, K. P.; Mansuy, D.; Hoa, G. H. B. *Biochem. J.* **1996**, *319*, 675−681.
(33) Good, N. E.; Winget, G. D.; Winter, W.; Connolly, T. N.; Izawa, S.; Singh, R. M. M. *Biochemistry* **1966**, *5*, 467−477.
(34) Totani, K.; Iizuka, T.; Shimada, H.; Makino, R.; Ishimura, Y. *Arch. Biochem. Biophys.* **1983**, *222*, 207−215.
(35) Denisov, I. G.; Grinkova, Y. V.; McLean, M. A.; Sligar, S. G. *J. Biol. Chem.* **2007**, *282*, 26865−26873.
(36) Berka, V.; Tsai, A. L. *Biochemistry* **2000**, *39*, 9373−9383.
(37) Clay, M. D.; Yang, T. C.; Jenney, F. E., Jr.; Kung, I. Y.; Cosper, C. A.; Krishnan, R.; Kurtz, D. M., Jr.; Adams, M. W.; Hoffman, B. M.; Johnson, M. K. *Biochemistry* **2006**, *45*, 427−438.
(38) Haynes, W. M. *CRC Handbook of Chemistry and Physics*, 93rd ed.; CRC Press: Boca Raton, FL, 2012; p 2664.
(39) Kavanagh, M. E.; Coyne, A. G.; McLean, K. J.; James, G. G.; Levy, C. W.; Marino, L. B.; de Carvalho, L. P.; Chan, D. S. H.; Hudson, S. A.; Surade, S.; Leys, D.; Munro, A. W.; Abell, C. *J. Med. Chem.* **2016**, *59*, 3272−3302.
(40) Cruce, A. A.; Lockart, M.; Bowman, M. K. *Methods Enzymol.* **2015**, *563*, 311−340.
(41) Goldfarb, D.; Bernardo, M.; Thomann, H.; Kroneck, P. M. H.; Ullrich, V. *J. Am. Chem. Soc.* **1996**, *118*, 2686−2693.
(42) LoBrutto, R.; Scholes, C. P.; Wagner, G. C.; Gunsalus, I. C.; Debrunner, P. G. *J. Am. Chem. Soc.* **1980**, *102*, 1167−1170.
(43) Mulks, C. F.; Scholes, C. P.; Dickinson, L. C.; Lapidot, A. *J. Am. Chem. Soc.* **1979**, *101*, 1645−1654.
(44) Yosca, T. H.; Rittle, J.; Krest, C. M.; Onderko, E. L.; Silakov, A.; Calixto, J. C.; Behan, R. K.; Green, M. T. *Science* **2013**, *342*, 825−829.
(45) Yosca, T. H.; Behan, R. K.; Krest, C. M.; Onderko, E. L.; Langston, M. C.; Green, M. T. *J. Am. Chem. Soc.* **2014**, *136*, 9124−9131.
(46) Green, M. T. *J. Am. Chem. Soc.* **2006**, *128*, 1902−1906.
(47) Hayakawa, S.; Matsumura, H.; Nakamura, N.; Yohda, M.; Ohno, H. *FEBS Lett.* **2013**, *587*, 94−97.
(48) Dumas, V. G.; Defelipe, L. A.; Petruk, A. A.; Turjanski, A. G.; Marti, M. A. *Proteins: Struct., Funct., Genet.* **2014**, *82*, 1004−1021.

DOI: 10.1021/jacs.7b08911
J. Am. Chem. Soc. 2017, 139, 17484−17499

Supplementary Information

Probing Ligand Exchange in the P450 Enzyme CYP121 from *Mycobacterium tuberculosis*: Dynamic Equilibrium of the Distal Heme Ligand as a Function of pH and Temperature

Andrew J. Fielding, Kednerlin Dornevil, Li Ma, Ian Davis, and Aimin Liu*
Department of Chemistry, University of Texas at San Antonio, San Antonio, TX 78249, United States

Spectroscopic characterization and K_D-value for imidazole binding to CYP121

In our initial efforts to purify CYP121 we observed two distinctly different low-spin (S = 1/2) signals in the as-isolated protein at pH 7.4 (50 mM Tris-HCl).[1] At low temperature and high microwave powers (4.5 K and 25.2 mW) a small population of a high-spin heme (S = 5/2) was also observed.[1] As our experiments were performed on a His_6-tagged protein, purified using a cobalt-metal affinity column and then eluted using an imidazole gradient. We suspected that the new low-spin signal could be due to remaining imidazole bound to the heme that was not adequately removed by the buffer exchange step using a G-25 size exclusion column. A red shift was observed in the Soret band for the as-isolated enzyme from 416 to 431 nm upon imidazole binding (Figure S1 panels A and B), which is consistent with Type II ligand-binding, in which imidazole is coordinating directly to the Fe(III)-heme. CYP121 was found to only weakly bind imidazole with a K_D-value of 55 ± 8 mM (Figure S1C). The as-isolated protein after the buffer exchange step also exhibited none of the spectral changes associated with imidazole (Imd) binding, (Figure S1D), this suggests that the second low-spin species was not an artifact of the purification process.

Figure S1

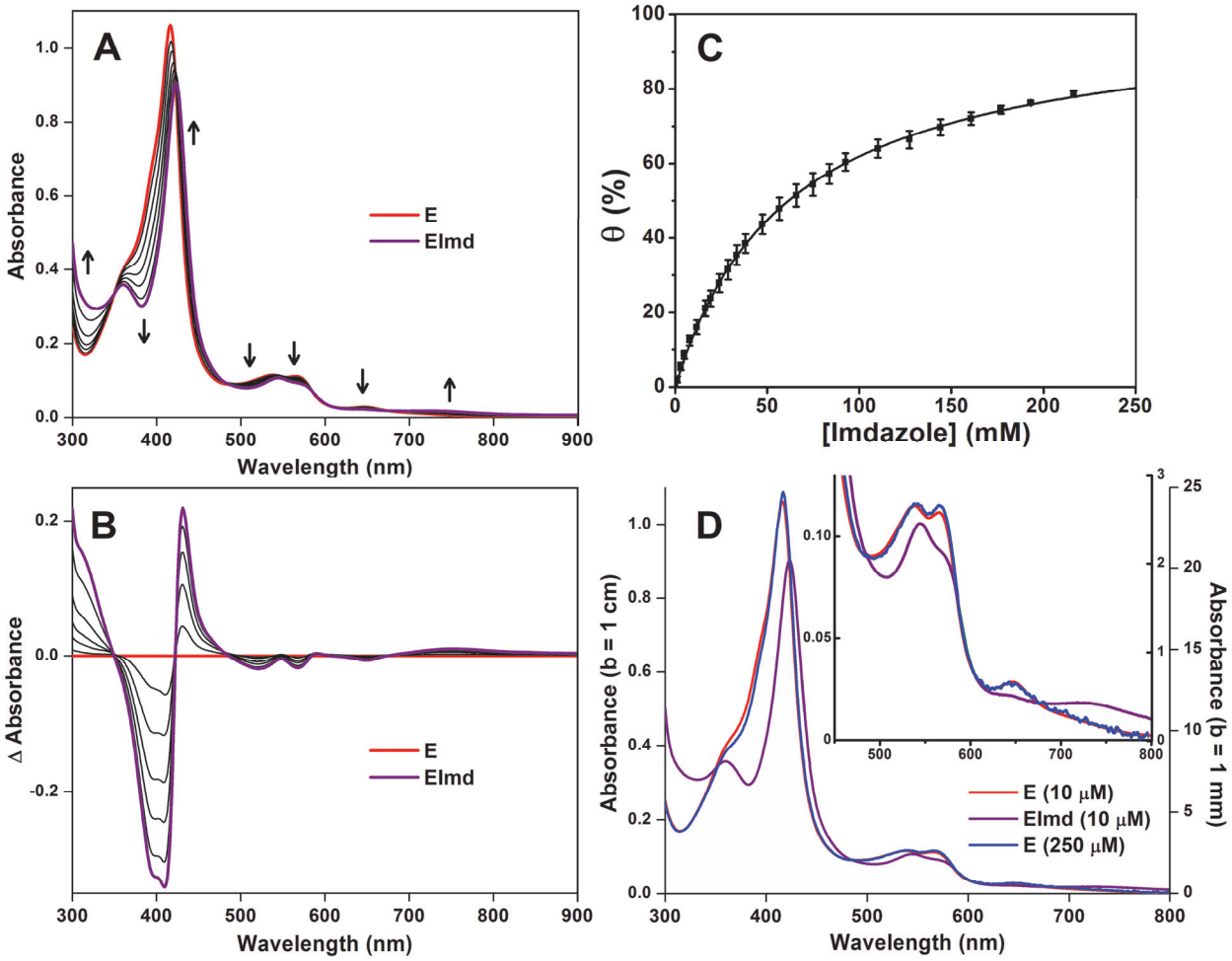

Figure S1. (A) UV-Vis titration of Fe(III)-CYP121 (**E**, 10 μM) with imidazole (Imd, 0–215 mM), in 150 mM HEPES buffer pH 7.5. The UV-Vis spectra of the **E** and [Fe(III)CYP121(Imd)] (**E**Imd) are distinct. (B) Difference spectra subtracting the spectrum of **E** from spectrum of the **E**Imd. Maximum change in amplitudes observed in the difference spectra at 300, 395, 408, 431, 517, 566, 645, and 745 nm with isosbestic points at 349, 422, 485, and 675 nm upon imidazole binding. (C) The K_D-value was determined by following the change in absorption between 408 and 431 nm over the course of the titration, K_D = 55 ± 6 mM imidazole. (D) Comparison of UV-Vis spectrum of diluted sample of **E** (10 μM heme), and **E**Imd, containing 10 μM heme and 180 mM imidazole. Compared to concentrated **E** (250 μM) in 50 mM Tris-HCl buffer pH 7.6 with 5% glycerol. Spectra of the dilute samples containing 10 μM **E** were acquired using a 1 cm quartz cuvette. The spectrum of the concentrated 250 μM sample was collected using a Nanodrop One UV-Vis spectrophotometer from Thermo Fisher Scientific with a 1 mm path-length.

Figure S2

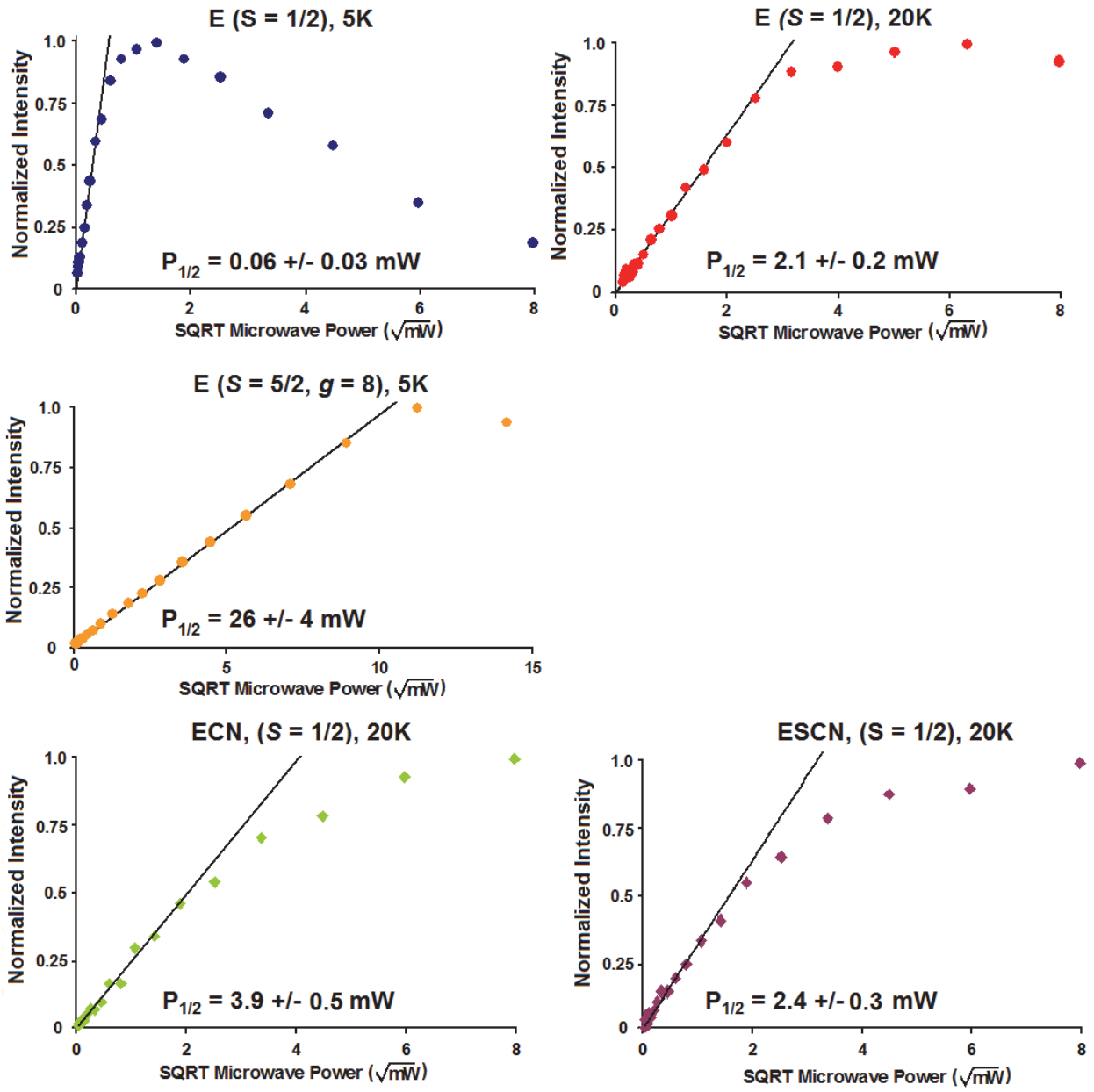

Figure S2. EPR temperature and microwave power saturation experiments performed on: (top) the low-spin **E** (ls-**E2**) sample prepared at pH 9.5 at (left) 5 K and (right) 20 K. (Middle) the high-spin **E**, at 5 K monitoring the EPR signal intensity at g = 8. (Bottom, left) **E**CN, and (Bottom, right) **ES**CN at 20 K. While the high-spin signal was most easily observed at 5 K and relatively high microwave power (25.3 mW), the low-spin signals were saturated at the low temperature and high power conditions, leading to a distorted spectrum and non-quantitative signal intensities. The $P_{1/2}$ values were measured by fitting plot of signal intensity as a function of microwave power with hyperbolic equation, plots not shown.

Figure S3

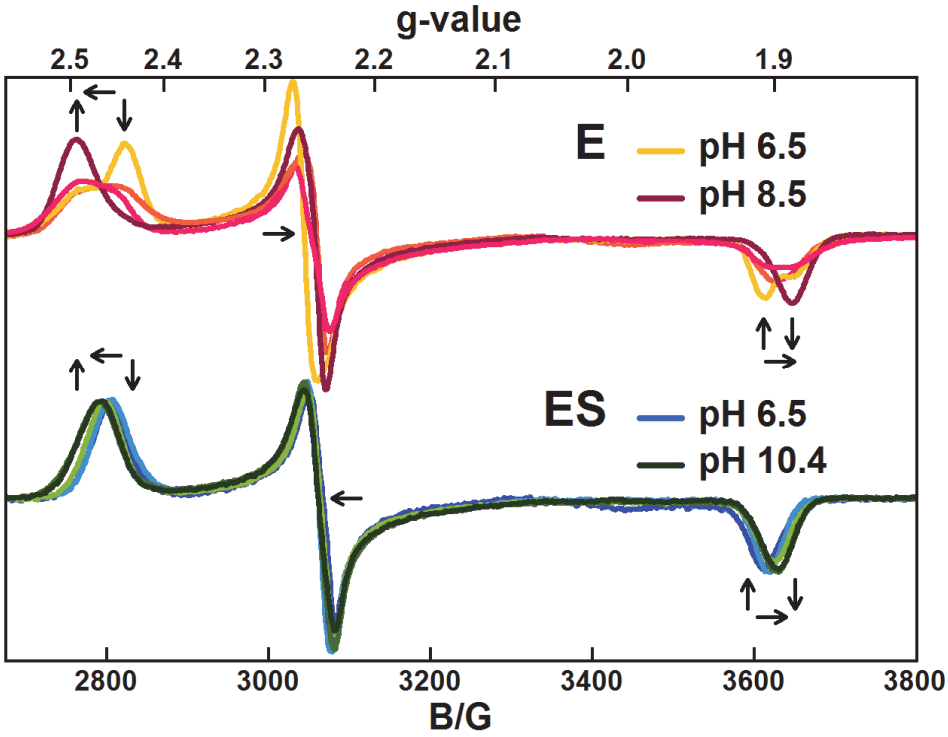

Figure S3. EPR spectra of the low-spin signals from the as-isolated enzyme Fe(III)-CYP121 (pH 6.5 to 8.5), and enzyme-substrate complexes, [ls-Fe(III)-CYP121(cYY)] (pH 6.5 to 10.4), prepared in different pH buffers. Arrows show the direction of change in the different observed EPR features upon increasing the pH from 6.5 to 10.4. Spectra collected at 20 K, 2.0 mW microwave power, 100 kHz modulation frequency, and 6 G modulation amplitude. Spectra have been normalized to the same intensity by double integration to account for different concentration of low-spin Fe(III)-heme in each sample for better comparison of spectral features.

Figure S4

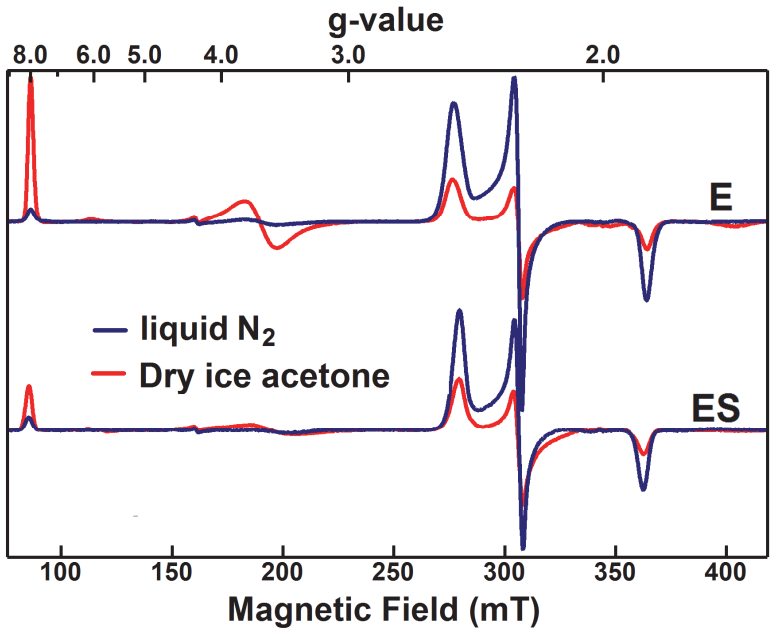

Figure S4. EPR spectra of Fe(III)-CYP121 **E** and [Fe(III)-CYP121(cYY)] **ES** complex at pH 10.4. Samples prepared initially at 22 °C and then frozen by various methods: by (blue) slow submersion in liquid nitrogen (-196 °C) and (red) rapid submersion in dry ice acetone bath (-78 °C). **ES** complexes were formed by incubating 285 μM CYP121 [heme] with 1.3 mM cYY. Spectra were collected at 4.5 K, 25 mW microwave power, 100 kHz modulation frequency, and 6 G modulation amplitude.

Figure S5

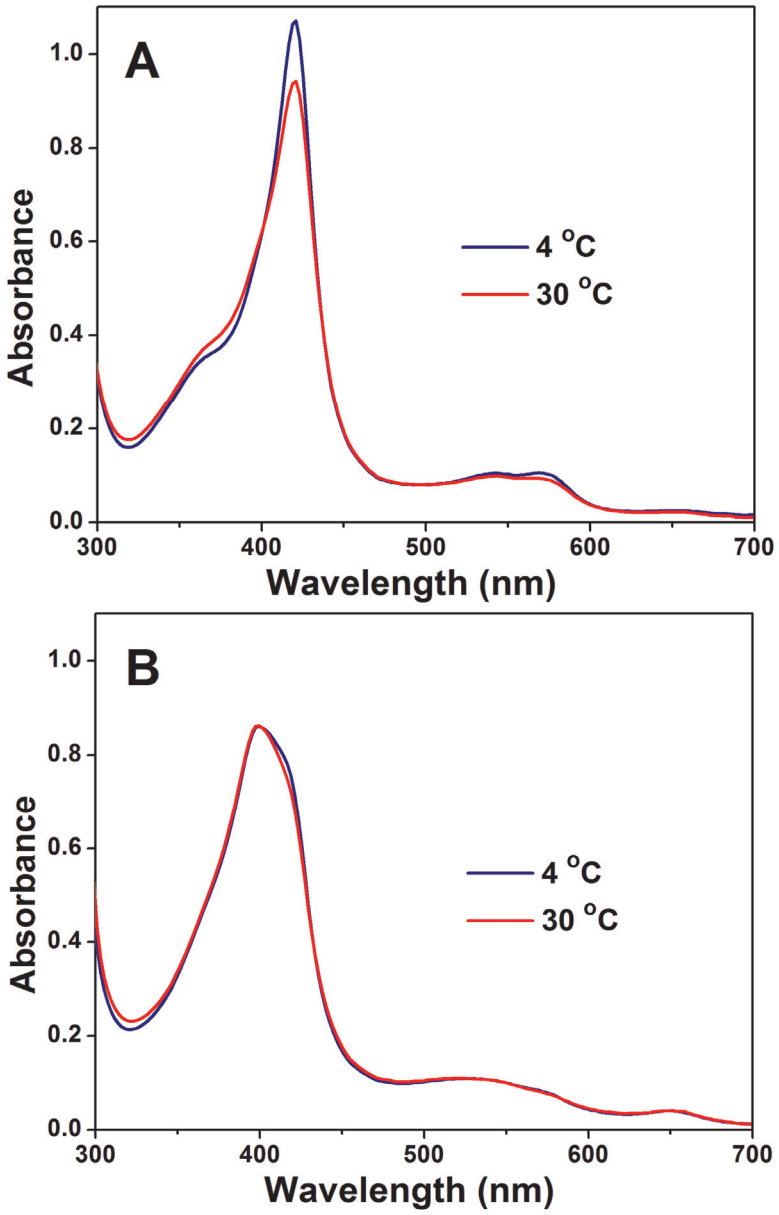

Figure S5. Temperature dependence of UV-Vis spectra for (A) Fe(III)-CYP121 (**E**, 10 μM [heme]) and (B) Fe(III)CYP121 (**ES**, 10 μM heme with 1680 μM cYY). Spectra were collected at 4 and 30 °C in 150 mM HEPES at pH 7.5. As the pK_a of HEPES buffer decreases by -0.14 units for every 10 °C, the pH of the HEPES buffer was adjusted to 7.5 at 4 and 30 °C prior to adding protein.

Figure S6

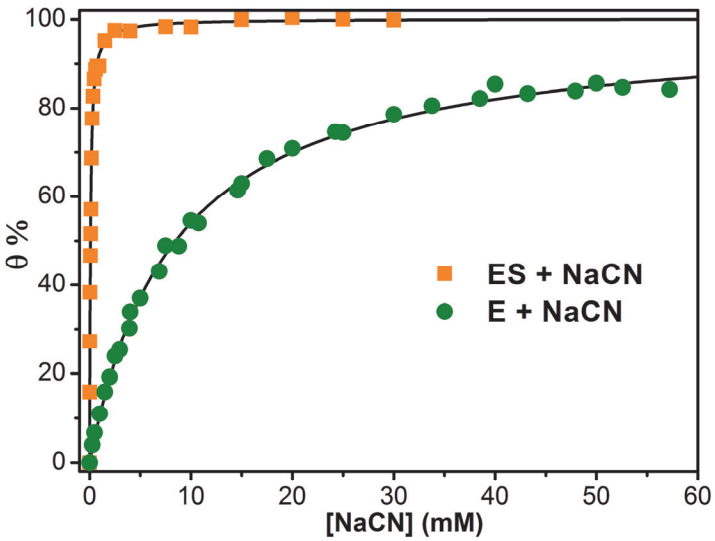

Figure S6. Titrations of **E** and **ES** with NaCN from Figure 3, at pH 7.5 in 150 mM HEPES buffer. Samples both contained 10 μM heme. **ES** was prepared by incubating **E** with 0.67 mM cYY. Data displayed as percent fraction bound (θ%). K_D^{CN} values for cyanide binding to **E** and **ES** are 8.8 ± 0.3 mM and 0.083 ± 0.006 mM NaCN, respectively (Table 4).

Figure S7

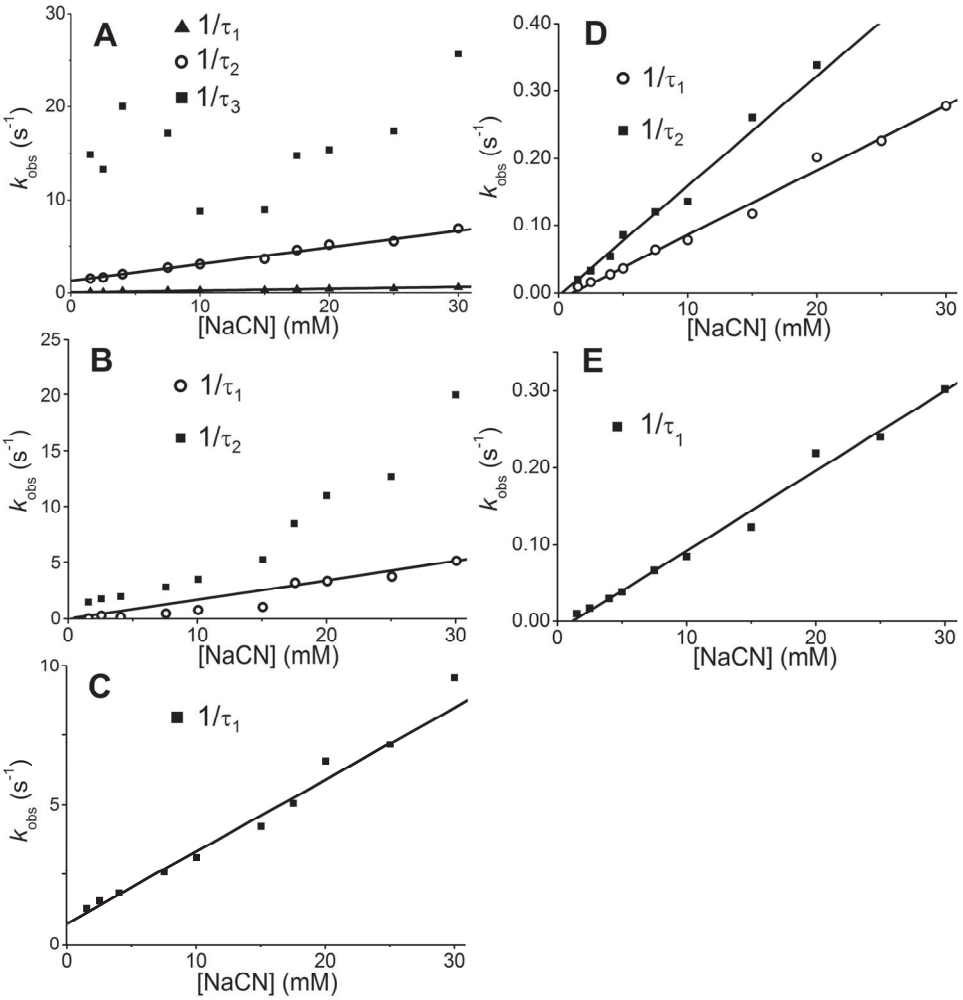

Figure S7. NaCN concentration dependence of observed rates from kinetic fitting of stopped-flow data monitoring the formation of **E**CN (left, Figure in 5A) and **ES**CN (right, Figure in 5B). Panels A, B and C show NaCN concentration dependence from fitting stopped-flow data for the formation of **E**CN to summed triple (A), double (B) or single (C) exponential equations. Panels D and E show fitting of stopped-flow traces monitoring the formation of **ES**CN to summed double (D), or single (E) exponential equations.

Figure S8

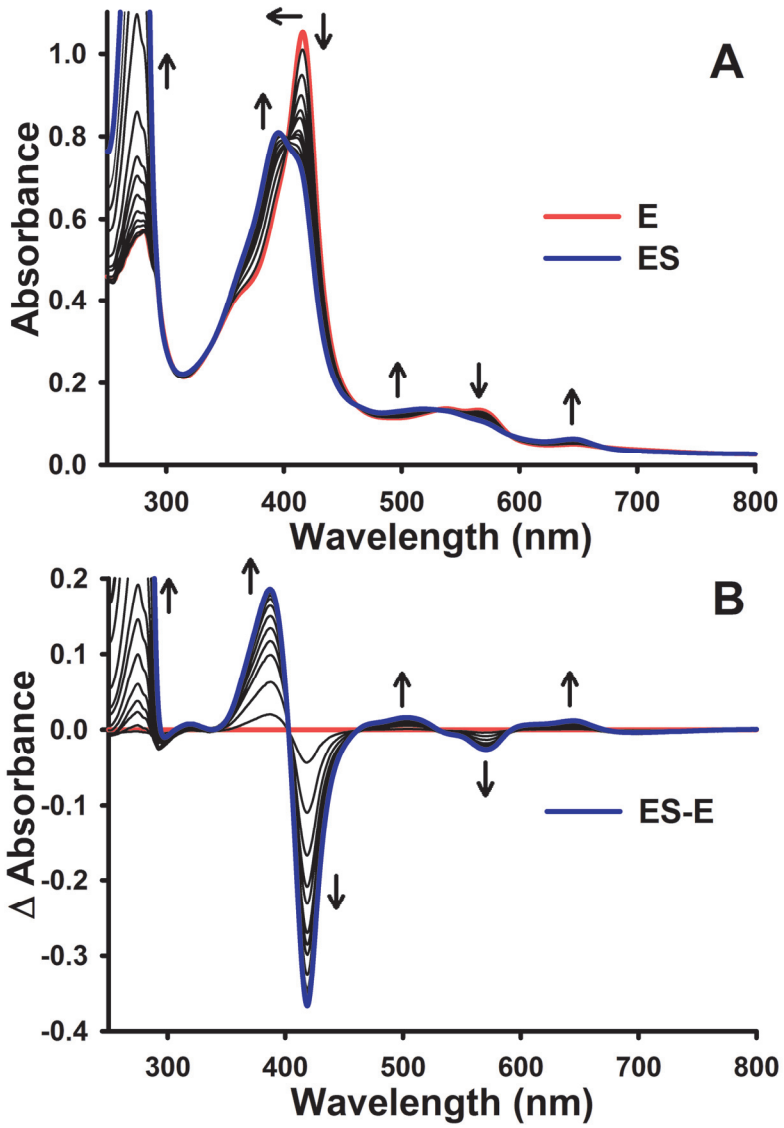

Figure S8. (A) Titration of Fe(III)-CYP121 (**E**, 9.5 μM [heme]) with cYY (0–530 μM cYY) to form **ES,** in 150 mM HEPES pH 7.5. (B) Difference spectrum, from subtracting the initial spectrum of CYP121 without substrate from the rest of the spectrum over the course of the titration. The plotted data were normalized for change in volume due to dilution effect with each successive addition of cYY. Titrations were monitored by following the amplitude difference between 386 and 419 nm over the course of the titration at pH-values ranging from 6.5 to 10.4 to determine the K_D^{cYY}-values (Figure 8). Increase in absorbance at 275 nm is from added cYY (Figure 7).[1-3]

Figure S9

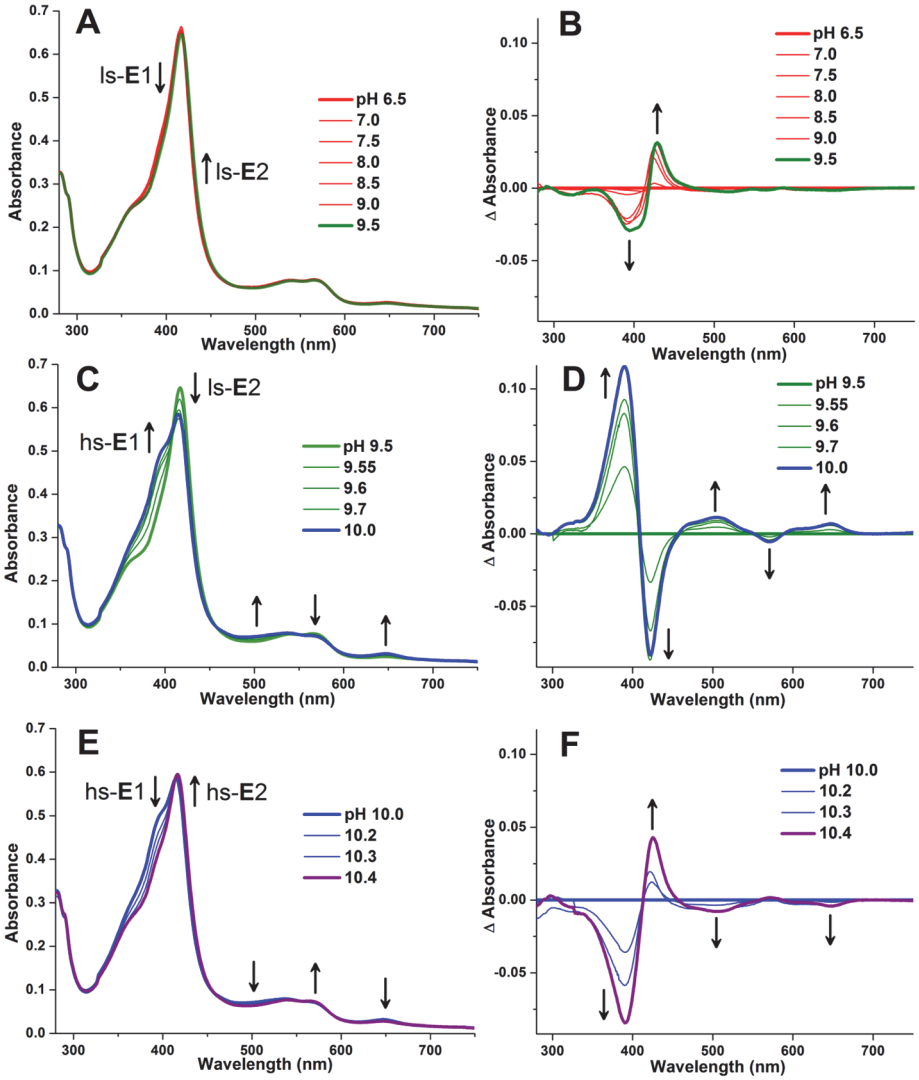

Figure S9. UV-Vis pH titration of Fe(III)-CYP121 (**E**, 6 μM heme). Absorbance spectra (left column) and difference spectra (right column) showing titrations data between pH 6.5 to 9.5 (A and B), pH 9.5 to 10 (C and D), and pH 10.0 to 10.4 (E and F). Samples prepared in 150 mM buffer described in materials and methods section at each pH.

Figure S10

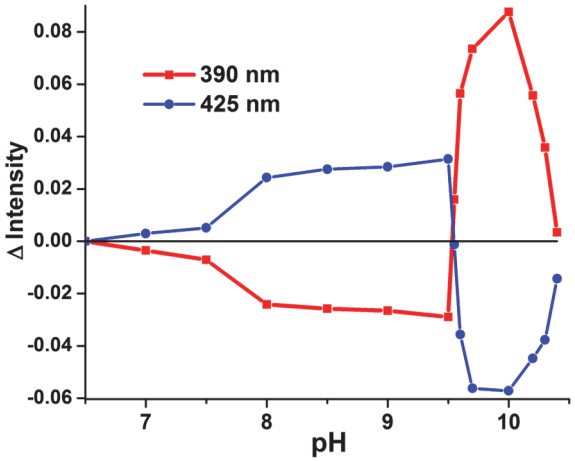

Figure S10. UV-Vis pH titration curves of Fe(III)-CYP121 (**E**, 6 μM heme), following change in absorbance at 390 and 425 nm, over the course of the titration shown in the previous figure (Figure S9).

Figure S11

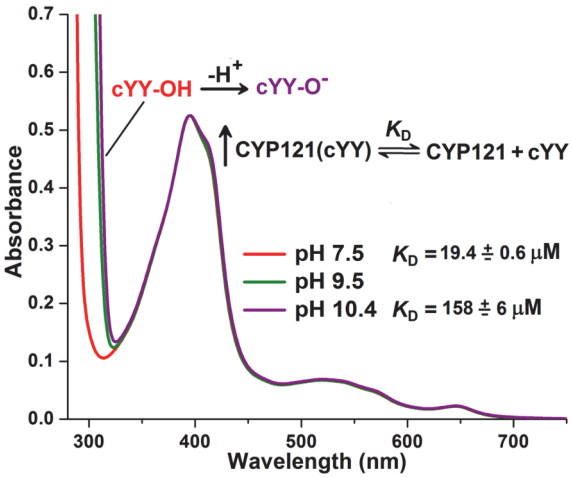

Figure S11. UV-Vis pH titration of [Fe(III)-CYP121(cYY)] (**ES**, 6 μM [heme] and 1.3 mM cYY).

Figure S12

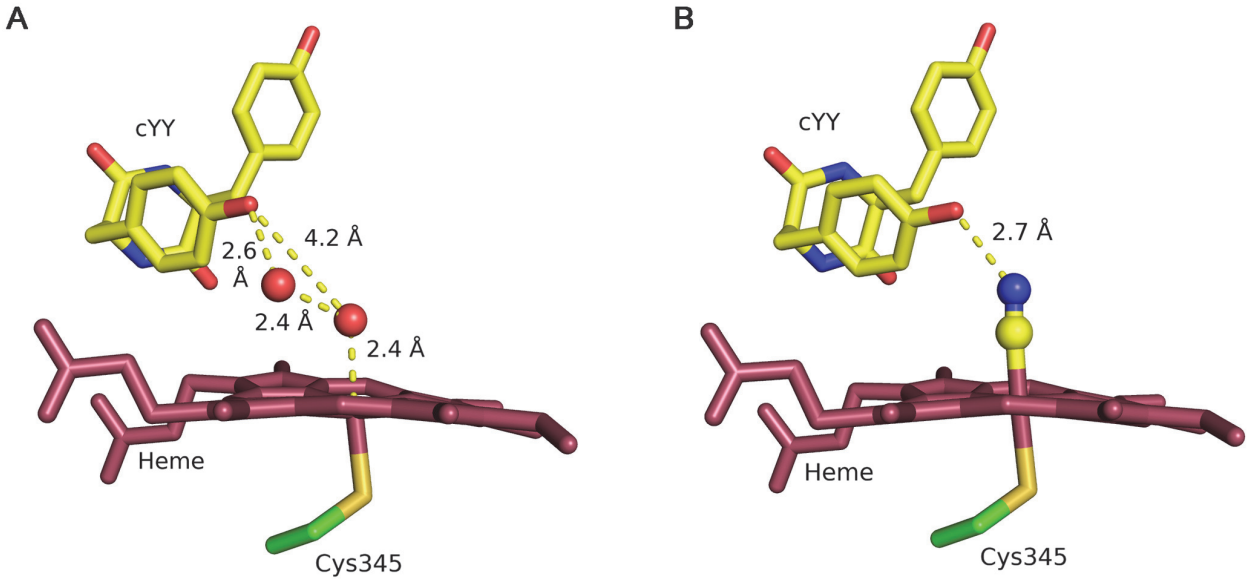

Figure S12. A side-by-side comparison of the CYP121 active site of the **ES** (A, from 3G5H.pdb, 1.4 Å resolution)[2] and **ES**CN (B, PDB entry: 5WP2, 1.4 Å resolution) complex structures.

Figure S13

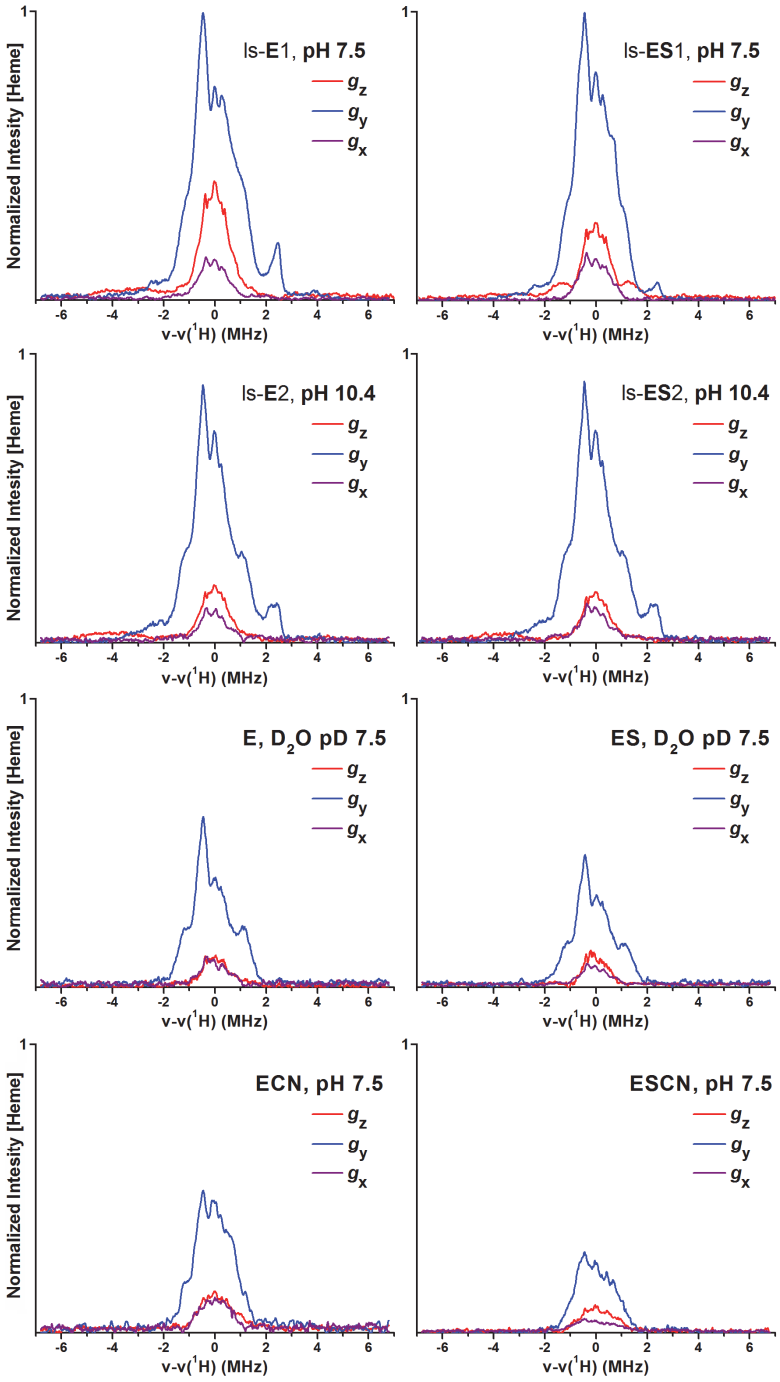

Figure S13. Comparison of the cw-ENDOR spectra of Fe(III)CYP121 (left column), and [Fe(III)-CYP121(cYY)] (right column) and in complex with cyanide; [Fe(III)CYP121(CN)] (bottom left), and [Fe(III)-CYP121(cYY)CN] (bottom right). Data shown for samples prepared in buffered solutions at pH 7.5, pH 10.4 or in D_2O (pD 7.5). Samples contained 1.0 to 1.3 mM CYP121 [heme], 1.7 mM cYY, 55 mM NaCN. Signal intensity has been normalized to concentration of heme in each sample determined by UV-Vis spectroscopy (ε_{416nm} = 110,000 M^{-1} cm^{-1}). Spectra were acquired at magnetic fields corresponding to *g*-values (g_z, g_y, and g_x) in the low-field, derivative and high-field features of each given species. Spectra have been centered at ^1H Larmor frequency for comparison. ^1H ENDOR spectra were collected under saturating conditions (Figure S2), at 20 K, 25.2 mW microwave power, and 60 W radio power with 100 kHz modulation depth.

Figure S14

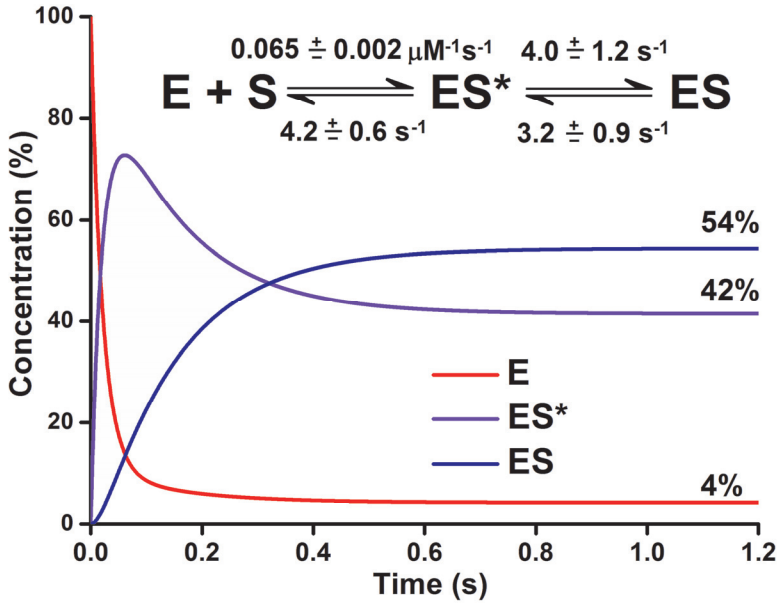

Figure S14. Simulation of time course for cYY (700 μM) binding to **E** (100 μM) using rate constants from stopped-flow cYY binding experiments.[1]

References

1. Dornevil, K. D.; Davis, I.; Fielding, A. J.; Terrell, J. R.; Ma, L.; Liu, A. *J. Biol. Chem.* **2017**, *292*, 13645–13657.
2. Belin, P.; Du, L. M. H.; Fielding, A.; Lequin, O.; Belin, P.; Jacquet, M.; Charbonnier, J.-B.; Lecoq, A.; Thai, R.; Courçon, M.; Masson, C.; Dugave, C.; Genet, R.; Pernodet, J.-L.; Gondry, M. *Proc. Natl. Acad. Soc. U.S.A.* **2009**, *106*, 7426–7431.
3. McLean, K. J.; Marshall, K. R.; Richmond, A.; Hunter, I. S.; Fowler, K.; Kieser, T.; Gurcha, S. S.; Besra, G. S.; Munro, A. W. *Microbiol.* **2002**, *148*, 2937–2949.